Published June 30, 2008

How ATP Inhibits the Open K_{ATP} Channel

Tim J. Craig, Frances M. Ashcroft, and Peter Proks

Henry Wellcome Centre for Gene Function, Department of Physiology, Anatomy and Genetics, University of Oxford, Oxford OX1 3PT, UK

ATP-sensitive potassium (K_{ATP}) channels are composed of four pore-forming Kir6.2 subunits and four regulatory SUR1 subunits. Binding of ATP to Kir6.2 leads to inhibition of channel activity. Because there are four subunits and thus four ATP-binding sites, four binding events are possible. ATP binds to both the open and closed states of the channel and produces a decrease in the mean open time, a reduction in the mean burst duration, and an increase in the frequency and duration of the interburst closed states. Here, we investigate the mechanism of interaction of ATP with the open state of the channel by analyzing the single-channel kinetics of concatenated Kir6.2 tetramers containing from zero to four mutated Kir6.2 subunits that possess an impaired ATP-binding site. We show that the ATP-dependent decrease in the mean burst duration is well described by a Monod-Wyman-Changeux model in which channel closing is produced by all four subunits acting in a single concerted step. The data are inconsistent with a Hodgkin-Huxley model (four independent steps) or a dimer model (two independent dimers). When the channel is open, ATP binds to a single ATP-binding site with a dissociation constant of 300 μM.

INTRODUCTION

ATP-sensitive potassium (K_{ATP}) channels couple cell metabolism to transmembrane potassium fluxes in many cell types (Ashcroft, 2005). They are important in the regulation of neuronal excitability (Liss et al., 1999; Hernandez-Sanchez et al., 2001; Miki et al., 2001; Yamada et al., 2001), neuronal degeneration (Liss et al., 2005), cardiac ischaemia and stress adaptation (Zingman et al., 2002; Liu et al., 2004; Kane et al., 2005), vascular smooth muscle tone (Miki et al., 2002), skeletal muscle fatigue (Gong et al., 2000), and hormonal secretion (Ashcroft et al., 1984; Reimann and Gribble, 2002; MacDonald et al., 2007). In pancreatic β cells, for example, closure of K_{ATP} channels in response to glucose metabolism depolarizes the plasma membrane, thereby triggering calcium influx and insulin release (Ashcroft et al., 1984). Accordingly, gain-of-function mutations in the genes encoding the β-cell K_{ATP} channel cause neonatal diabetes and loss-of-function mutations cause the converse disorder, congenital hyperinsulinism (Ashcroft, 2005; Hattersley and Ashcroft, 2005).

The K_{ATP} channel is an octameric complex of two types of membrane-protein subunit (Inagaki et al., 1995; Sakura et al., 1995). Kir6.2, a member of inwardly rectifying potassium channel family, forms a central tetrameric pore. Each Kir6.2 subunit associates with a regulatory protein, the sulphonylurea receptor (SUR1), in 4:4 stoichiometry (Clement et al., 1997; Mikhailov et al., 2005).

Metabolism is believed to regulate K_{ATP} channel activity primarily via changes in the concentrations of intracellular adenine nucleotides. Channel inhibition is produced by binding of ATP to Kir6.2 in a Mg-independent manner (Tucker et al., 1997; Gribble et al., 1998). Conversely, occupancy of the nucleotide-binding domains of SUR1 by MgADP stimulates channel activity, a circumstance that can be achieved either by direct binding of MgADP or by binding and subsequent hydrolysis of MgATP (Nichols et al., 1996; Tucker et al., 1997; Gribble et al., 1998; Zingman et al., 2001). Identification of the molecular mechanism by which the K_{ATP} channel is gated by ATP and MgATP/MgADP is therefore crucial for understanding how cell metabolism is linked to channel activity and thereby to the plasma membrane potential. This paper focuses on the mechanism of inhibition by ATP. This can be studied in isolation from nucleotide interactions with SUR1 by using Mg^{2+}-free solutions.

The K_{ATP} channel is spontaneously active in the absence of ATP: we refer to this as intrinsic gating (sometimes it is also referred to as ligand-independent gating). The single-channel kinetics are characterized by bursts of short openings and closings separated by long, nonconducting interburst intervals. Addition of ATP causes a marked reduction in burst duration and pronounced prolongation of the long closed states. ATP therefore interacts with all these states.

Analysis of ATP inhibition of macroscopic currents does not enable the interaction of ATP with the different states of the channel to be distinguished. It also cannot be reliably used to determine the stoichiometry of ATP inhibition, as many different models can be easily fit to the ATP concentration–response relationship.

Correspondence to Frances M. Ashcroft: frances.ashcroft@dpag.ox.ac.uk

The online version of this article contains supplemental material.

Abbreviations used in this paper: BR, burst ratio; D, dimer; HH, Hodgkin-Huxley; MWC, Monod-Wyman-Changeux; WT, wild type.

J. Gen. Physiol. Vol. 132 No. 1 131–144
www.jgp.org/cgi/doi/10.1085/jgp.200709874

Supplemental Material can be found at:
/content/suppl/2008/06/30/jgp.200709874.DC1.html

Published June 30, 2008

Although single-channel analysis overcomes some of these problems, analysis of the interaction of ATP with the long closed states of the channel remains a difficulty because there are multiple intrinsic long closed states whose distribution varies between individual channels; and because ATP-dependent stabilization of the closed states is otherwise too complex to model adequately at present. In this paper, we therefore focus on the interaction of ATP with the channel open state.

Several previous single-channel studies have examined the interaction of ATP with the channel open state and have concluded that ATP destabilizes the channel open state and thus promotes channel closure (Gillis et al., 1989; Nichols et al., 1991; Davies et al., 1992; Drain et al., 1998; Trapp et al., 1998; Fan and Makielski, 1999; Li et al., 2002). They have also shown that there is very little effect of ATP on the short closed state (Alekseev et al., 1998; Trapp et al., 1998; Li et al., 2002), indicating that the reduction in the burst duration is primarily due to the interaction of ATP with the channel open state. Consequently, the burst duration can be used to analyze how ATP interacts with the open state.

Single-channel analysis in several previous studies made the assumption that channel closure resulted from interaction of one ATP molecule with the open state (Trapp et al., 1998; Li et al., 2002). However, since each Kir6.2 subunit possesses an inhibitory ATP-binding site (Markworth et al., 2000; Antcliff et al., 2005) and the K_{ATP} channel has four Kir6.2 subunits (Clement et al., 1997), up to four ATP molecules could bind to the open state. The relationship between the number of ATP molecules bound and pore closure is unclear. More recently, Abraham et al. (2002) and Selivanov et al. (2004) assumed a kinetic model with four independent binding sites for ATP; despite the assumption of independence, the best fit of ATP dose–response curves required that more than one (at least two out of four) binding sites had to be occupied to induce channel closure.

In this paper, we describe a method for analyzing the single-channel kinetics of K_{ATP} channels containing different numbers of wild-type subunits and subunits with a mutated ATP-binding site. We use this method to determine the mechanism by which ATP interacts with the open state and thereby facilitates the closure of the channel pore. We conclude that the data can be described well by the Monod-Wyman-Changeux model.

MATERIALS AND METHODS

Molecular Biology

Concatenated Kir6.2 tetramers were engineered by stepwise addition of monomeric subunits, using the compatibility of BglII and BamHI restriction endonuclease sites. Wild-type Kir6.2 monomers were produced by standard PCR techniques. The Kir6.2ΔC monomer had a C-terminal deletion of 36 amino acids (ΔC36) (Tucker et al., 1997), a BamHI site at the 5′ end, and a BglII site at the 3′ end. For the first (N-terminal) Kir6.2 subunit, a Kozak ribosome binding sequence was engineered at the 5′ end, and for the final (C-terminal) subunit, a stop codon was inserted at the 3′ end. Glycine residues were also engineered into the subunits to extend the linker region between subunits: two glycines before the 3′ restriction site in the first subunit; two glycines after the 5′ restriction site and two glycines before the 3′ restriction site in the central subunits; two glycines after the 5′ restriction site in the final subunit. This results in an intersubunit linker of GGRSGG. All tetramers were constructed using the cloning vector pGEMT-Easy, before being subcloned into pBF vector for cRNA production.

To construct the Kir6.2 tetramer, the first subunit was inserted into pGEMT-Easy using the 5′-A overhangs, according to the vector protocol (Promega). For each subsequent subunit addition, the construct was cut with BglII, and the subunit, cut with BamHI and BglII, was ligated in to the BglII-cut construct. If the subunit is inserted in the correct orientation, the 5′ BamHI site is lost in the ligation process, leaving a 3′ BglII site, thus allowing addition of the next subunit in the same way. Mutant K185E subunits were produced by standard site-directed mutagenesis and inserted into the tetramer at the desired points by the same technique. A similar approach was taken by Wang et al. (2007).

Oocyte Handling

All animal studies were conducted in accordance with UK Home Office regulations and local ethical procedures. Female *Xenopus laevis* were anaesthetized with MS222 (2 g/liter added to the water). One ovary was removed via a mini-laparotomy, the incision was sutured, and the animal was allowed to recover. Once the wound was completely healed, the second ovary was removed in a similar operation and the animal was then killed by decapitation while under anesthesia. Immature stage V–VI *Xenopus* oocytes were incubated for 2 h with 1 mg/ml collagenase (type A; Boehringer Mannheim) and manually defolliculated. Oocytes were injected with ~0.04 ng mRNA encoding Kir6.2 or Kir6.2ΔC26 tetramer and ~2 ng SUR1 (giving 1:50 ratio). Isolated oocytes were maintained in tissue culture and studied 1–4 d after injection.

Electrophysiology

Patch electrodes were pulled from thick-walled borosilicate glass (GC-150; Harvard Electronics). Single-channel activity of 1–20 min duration was recorded at −60 mV, filtered at 5 kHz, and digitized at 50 kHz using an Axopatch 200B patch-clamp amplifier (Axon Instruments) and pClamp software (Axon Instruments). All experiments were done at room temperature (20–22°C). The pipette solution contained (in mM) 140 KCl, 1.2 $MgCl_2$, 2.6 $CaCl_2$, 10 HEPES (pH 7.4 with KOH). The internal (bath) solution contained (in mM) 107 KCl, 1 K_2SO_4, 10 EGTA, 10 HEPES (pH 7.2 with KOH) and K_2ATP as indicated. Before and after application of ATP, the patch was exposed to ATP-free (control) solution for 1 min. During long recordings in high ATP solution, if channel activity was very low, ATP-free solution was applied at intervals to check for channel rundown.

The data were analyzed using a combination of Clampfit, Origin (OriginLab Corporation) and in-house software. Dwell-time histograms were constructed and analyzed at a resolution of 0.15 ms as described previously (Davies et al., 1992). Open time distributions were fit with a single exponential; up to four exponentials were fitted to dwell-time distributions. Burst durations were determined using the criterion for the critical time described by Magleby and Pallotta (1983):

$$a_f e^{-t_{crit}/\tau_f} = \sum_i^n a_{si}(1 - e^{-t_{crit}/\tau_{si}}), \quad (1)$$

where a_f and τ_f are the area and the mean lifetime of the intraburst state (which corresponds to the component with the shortest mean lifetime in the distribution of closed times), and a_{si} and

Published June 30, 2008

τ_{si} are the areas and mean lifetimes of the interburst states (corresponding to all other components in the distribution of closed times). The index i refers to the number of interburst components; in our experiments, i varied between 1 and 3.

To distinguish between different kinetic models, data analysis was performed on the mean burst ratios, BR (the ratio of the mean burst duration in the absence of ATP to that in the presence of ATP). To assess the accuracy of the mean BR obtained by Magleby and Pallotta's method, BR was also determined by an independent method, described by Fang et al. (2006). There was no significant difference between the mean BRs obtained by these two methods (see online supplemental material, http://www.jgp.org/cgi/content/full/jgp.200709874/DC1).

The mean burst duration in ATP-free solution ($\tau_B(0)$) was taken as an average of that measured before and after application of ATP. In this paper, we calculate the mean burst duration as follows: first we measured the mean burst duration in three to five single-channel patches, and then we calculated the average of these mean burst durations.

The value of the mean burst duration obtained by averaging all burst events can be distorted by a "missed events" error, which results from missing very short solitary openings (as these also contribute to the burst pdf; e.g., Shelley and Colquhoun, 2005). In this study, however, such errors will be small. Both homomeric and heteromeric K_{ATP} channels exhibited quasi-monoexponential distributions of open times over the range of ATP concentrations of up to 5 mM. A similar result for homomeric wild-type K_{ATP} channels was previously obtained by Li et al. (2002). The mean open time ranged from 0.4 to 2 ms, which is well above the limit of detectability in our system. Thus the number of very brief openings that go undetected is likely to be very small compared with the total number of bursts. The largest error can be expected for unconnected wild-type channels, for which the reduction in open time by ATP is largest (Fig. S13 C). However, the value of K_O (or m) obtained from fitting the mean burst durations of these channels (Eq. 11) was similar to that obtained (independently) from fitting the mean open time (which was corrected for missed events with Eq. S3 as described by Davies et al., 1992) using Eq. S4 (see Table I). This indicates that errors arising from a failure to detect very brief openings (even for this limiting case) are likely to be small.

The intrinsic rate constants a,b,c in Scheme 1 were calculated from the mean open time $\tau_O(0)$, the short intraburst closed time $\tau_F(0)$, and the mean burst duration $\tau_B(0)$ in the absence of ATP using the following equations:

$$1/\tau_F(0) = b \tag{2}$$

$$1/\tau_O(0) = a + c \tag{3}$$

$$1/\tau_B(0) = \frac{1+\frac{a}{b}}{c}. \tag{4}$$

Macroscopic currents were recorded from giant inside-out patches at −60 mV and 20–22°C. Currents were filtered at 0.15 kHz and digitized at 0.5 kHz. The pipette and internal solutions were the same as those used in the single-channel studies. ATP concentration–response curves were fit with the Hill equation:

$$\frac{I(ATP)}{I(0)} = p + \frac{1-p}{1+\left(\frac{[ATP]}{IC_{50}}\right)^h}, \tag{5}$$

where $I(ATP)$ and $I(0)$ are the mean values of the K_{ATP} current in the presence and absence of the nucleotide, $[ATP]$ is the ATP concentration, IC_{50} is the ATP concentration at which inhibition is half maximal, h is the slope factor (Hill coefficient), and p is the fraction of unblocked current (pedestal) at saturating ATP concentrations (i.e., where all ATP-binding sites are occupied by nucleotide). For most types of K_{ATP} channel, channel activity at ATP concentrations >1 mM was determined by single-channel recording at high gain, where the background leak current could be clearly distinguished. Background currents determined in this way were extremely small. Thus they were regarded as negligible in those cases where the fraction of ATP-resistant current was too large to employ single-channel analysis (for example, tetrameric constructs with four or three mutant subunits). To control for possible rundown of channel activity, $I(0)$ was taken as the mean of the conductance in control solution before and after ATP application. Each data point represents the mean ± SEM of n patches.

Online Supplemental Material

The online supplemental material is divided into four parts (available at http://www.jgp.org/cgi/content/full/jgp.200709874/DC1). In the first part, which includes Figs. S1–S10 and Table S1, we compare the analysis of the mean burst ratios determined by the Magleby and Pallotta method (1985) with that of Fang et al. (2006). In the second part, we compare the ATP sensitivity of connected tetramers in macroscopic and single-channel recordings (Fig. S11). In the third part, we present the data on the ATP dependence of the burst ratio for K_{ATP} channels containing unconnected Kir6.2 subunits (Fig. S12). In the fourth part, we compare the macroscopic and single-channel properties of homomeric wild-type K_{ATP} channels formed from connected and separate Kir6.2 subunits (Fig. S13).

RESULTS

Connected Kir6.2 Tetramers

To assess how ATP interacts with the open state of the K_{ATP} channel, we studied channels containing various combinations of wild-type (WT) and mutant (M) Kir6.2 subunits. The K185E mutation was selected because it has been extensively characterized in previous studies (Reimann et al., 1999; John et al., 2003; Ribalet et al., 2003; Wang et al., 2007) and it severely reduces ATP inhibition without altering intrinsic gating (i.e., that in the absence of ATP). Residue K185 is predicted to reside within the ATP-binding site based on molecular modeling studies (Trapp et al., 2003; Antcliff et al., 2005).

Coinjection of a mixture of wild-type and mutant Kir6.2 mRNAs produces a mixed population of channels containing variable numbers of wild-type and mutant subunits. However, it does not constrain the subunit stoichiometry or position. We therefore constructed connected tetramers. As Fig. 1 shows, the tetramers contained between zero and four mutant subunits. To address the possibility of asymmetry in intersubunit interactions, we made two constructs with 2WT:2M stoichiometry: cis, in which wild-type and mutant subunits reside next to each other and trans, in which wild-type and mutant subunits face one another across in the assembled tetramer.

Three Major Types of Gating Models

ATP binds to the cytosolic domain of Kir6.2 (Drain et al., 1998; Tucker et al., 1998) and induces a conformational

Published June 30, 2008

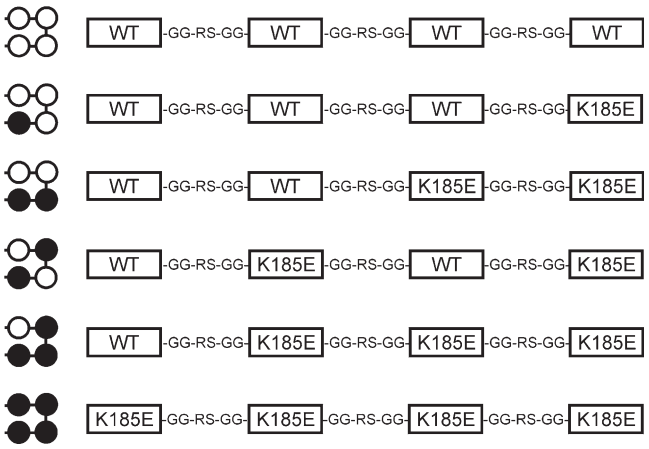

Figure 1. Schematic representation of connected tetramers. Schematic representation of the six tetrameric constructs employed. The distribution of wild-type (WT) and mutant K185E subunits is shown, together with the connecting amino acids. The arginine-serine (RS) in the connecting regions is supplied by the fused BglII and BamHI sites used in cloning. Open circles, wild-type Kir6.2 subunits; filled circles, Kir6.2-K185E subunits.

change(s) that that leads to stabilization of the closed conformation. Because there are four subunits, there are four ATP-binding sites per tetrameric channel. These could operate independently or in concert. Thus three types of models could describe the gating of the K_{ATP} channel (Fig. 2), in which the "gating unit" has one, two, or four ATP-binding sites and each K_{ATP} channel tetramer has four ($4GU_1$), two ($2GU_2$), or one (GU_4) gating unit, respectively (the subscript in each term refers to the number of ATP-binding sites within the gating unit). In all models, the gating units are considered to alternate between "active" (open) and "inactive" (closed) conformations. We further assume that transition of any one gating unit to its "inactive" conformation (strongly promoted by ATP binding to that unit) closes the pore. This terminates the burst and facilitates entry into the long closed states.

First, it is possible that each cytosolic domain of the Kir6.2 tetramer operates independently so that the channel may be considered to have four gating units ($4GU_1$). Thus, ATP binding to a single Kir6.2 subunit promotes channel closure (Fig. 2 A). In the simplest case, each Kir6.2 subunit behaves independently: i.e., ATP binds independently to the cytosolic domain of each Kir6.2 subunit, producing a conformational change that is independent of the ligand-binding state of all other subunits, and leads to closure of the channel pore. The channel will be closed as long as one gating unit is in the "closed" conformation; all four gating units must be in "open" conformation for the channel to be open. This mechanism is similar to that originally described by Hodgkin and Huxley for gating of voltage-dependent channels (Hodgkin and Huxley, 1952). It has also been proposed previously for K_{ATP} channels (Enkvetchakul et al., 2000).

However, studies of the intrinsic burst duration (Drain et al., 2004) and intrinsic interburst intervals (Fang et al., 2006) are inconsistent with this idea. Instead the data suggest that the four cytosolic domains of the channel may not function independently but operate together as a single gating unit (GU_4). In this case, we will assume that ATP binds to each subunit independently and makes an additive contribution to the free energy of the open or closed states (Fig. 2 B). This is known as the Monod-Wyman-Changeux model (Monod et al., 1965).

Finally, molecular dynamics simulations suggest that the K_{ATP} channel may operate as a dimer of dimers (Haider et al., 2005a). In this case, the channel would have two gating units formed by two opposing (or adjacent) Kir6.2 subunits ($2GU_2$). In the simplest case, binding of ATP to all four sites is independent; the effects of binding of two ATP molecules to one gating unit are additive; and the movements of the two gating units are independent. The channel will be closed as long as one gating unit (i.e., one dimer) is in the closed conformation; both dimers must be in the open conformation for the channel to be open. We refer to this as the dimer model.

For all models, the effects of ATP binding on the free energy of the open state are additive. However, binding of a single ATP will have the greatest effect in the case of the Hodgkin-Huxley (HH) model, and the least effect in the case of the MWC model.

To determine which model most closely describes the effect of ATP on the open state of the channel, it is necessary to have an ATP-dependent parameter that can be reliably determined from the experiment, and whose ATP dependence differs between the three models described above. Previous single-channel studies have characterized the ATP dependence of the mean open time and the mean burst duration (Davies et al., 1992; Trapp et al., 1998; Fan and Makielski, 1999; Li et al., 2002). Of these two parameters, the mean burst duration shows a dramatically greater dependence on ATP than the mean open time (e.g., 0.6 mM ATP reduces the former ~32-fold and the latter ~2.5-fold; Li et al., 2002). We therefore used the mean burst duration and its dependence on ATP as a probe to determine which kinetic model best describes ATP-dependent closure of the K_{ATP} channel.

The gating of the β-cell K_{ATP} channel can be well described by a kinetic scheme with a single open state (O), one intraburst closed state (C_S), and several interburst closed states (e.g., Alekseev et al., 1998; Trapp et al., 1998; Enkvetchakul et al., 2000; Fang et al., 2006). In this study, we use a simplified kinetic scheme with a single interburst closed state (C_F), as our analysis is not concerned with transitions between interburst closed states:

$$C_F \underset{b}{\overset{a}{\rightleftharpoons}} O \underset{d}{\overset{c}{\rightleftharpoons}} C_S$$

(SCHEME 1)

Published June 30, 2008

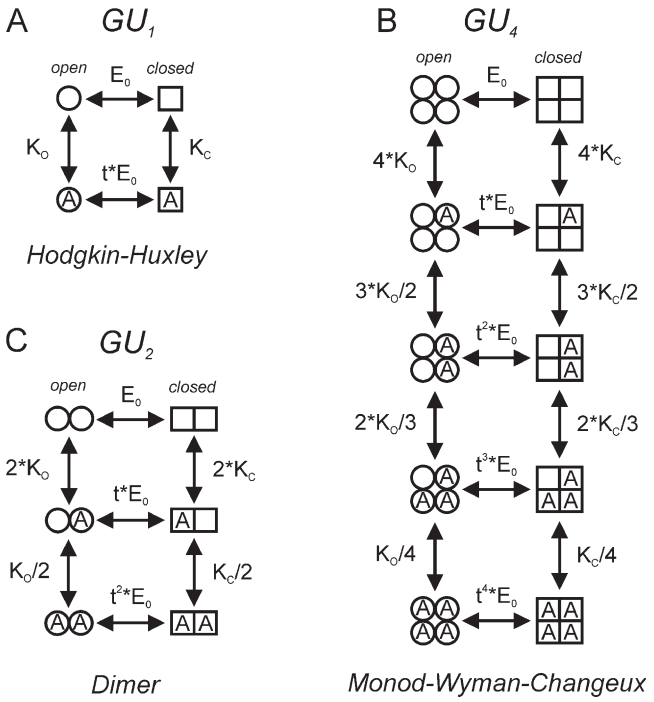

Figure 2. Three types of models for K_{ATP} channel gating. Schematic representation of the different types of models. (A) Four independent gating units ($4GU_1$), each formed by one Kir6.2 subunit. (B) One gating unit formed by all four Kir6.2 subunits (GU_4). (C) Two independent gating units, each formed by two Kir6.2 subunits ($2GU_2$). In each case, the transitions between open and closed states are shown for a single gating unit. Each Kir6.2 subunit can be either in an "open" (circle) or "closed" (square) conformation. It is assumed that ATP binds independently to all subunits and A indicates the presence of bound ATP. K_O and K_C are the binding constants to the open and closed states, respectively. E_O is the equilibrium gating constant in the absence of ATP. The term t indicates the change in the equilibrium gating constant due to bound ATP. It is assumed that ATP binding has an additive effect on the energy of the gating unit in both open and closed conformations.

where a and b are the rate constants for transitions between the intraburst states O and C_F, and c and d are the rate constants for transitions between the open state and interburst closed state C_S.

In principle, all three states can bind ATP, producing the corresponding ATP-bound states O_A, C_{FA}, and C_{SA}. Several earlier studies (Gillis et al., 1989; Davies et al., 1992; Trapp et al., 1998; Fan and Makielski, 1999; Li et al., 2002) assumed that interaction of ATP with the channel open state leads directly to K_{ATP} channel closure (i.e., that occupancy of the open state O_A was essentially zero). However, studies on mutant channels clearly showed that ATP-bound open states can contribute significantly to channel activity (Enkvetchakul et al., 2001; Wang et al., 2007). Thus, a realistic kinetic scheme should also include three ATP-bound states, as shown below (Colquhoun, 1998):

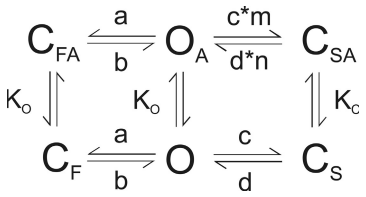

(SCHEME 2)

where K_O is the equilibrium binding constant for ATP binding to intraburst states (O, C_F) and K_C is the equilibrium binding constant for ATP binding to the interburst long closed states (C_S). Because the effect of ATP on intraburst closed states is very small (Alekseev et al., 1998; Trapp et al., 1998; Li et al., 2002), for simplicity, we assume that intraburst transitions (i.e., rate constants *a, b*) are unaffected by the nucleotide; we also assume they are the same for all three models shown in Fig. 2. In contrast, ATP substantially affects the rates of transitions between open and interburst closed states. Thus the rate constants governing transitions between the ATP-bound open state O_A and ATP-bound interburst closed state C_{SA} must include proportionality coefficients (*m, n*) that describe how much the rate of closure, or opening, respectively, is altered when ATP is bound (i.e., *c*m, d*n*).

The right side of the Scheme 2 corresponds to the allosteric cycle for binding of one ATP molecule in Fig. 2, where E_O *(=c/d)* is the equilibrium gating constant for transitions between states O and C_S and t *(=m/n)* is the transduction coefficient for the effect of ATP binding on this reaction. Since ATP is a K_{ATP} channel antagonist, it must bind with higher affinity to the interburst closed state (Cs in Scheme 2) than to the open state ($K_C > K_O$). From the principle of microscopic reversibility $K_C = t^*K_O$, and thus $t > 1$.

The mean burst durations for the models shown in Fig. 2 can now be fully determined from the rate constants in Scheme 2 and the bulk ATP concentration ([ATP]). The general formula for calculation of the mean burst duration τ_B is (Colquhoun and Hawkes, 1982):

$$\tau_B = \varphi_B(I - G_{AB}G_{BA})^{-1}(-Q_{AA}^{-1})(I - Q_{AB}Q_{BB}^{-1}G_{BA})u_A. \quad (6)$$

Using Eq. 6, the mean burst durations for the three gating models shown in Fig. 2 (which are expanded from Scheme 2) can be expressed as:

$$\frac{1}{\tau_{B,HH}([ATP])} = \frac{4*c*(1+m_{HH}*K_{O,HH}*[ATP])}{(1+F)*(1+K_{O,HH}*[ATP])} \quad (7)$$

$$\frac{1}{\tau_{B,MWC}([ATP])} = \frac{c*(1+m_{MWC}*K_{O,MWC}*[ATP])^4}{(1+F)*(1+K_{O,MWC}*[ATP])^4} \quad (8)$$

$$\frac{1}{\tau_{B,D}([ATP])} = \frac{2*c*(1+m_D*K_{O,D}*[ATP])^2}{(1+F)*(1+K_{O,D}*[ATP])^2}, \quad (9)$$

Published June 30, 2008

where $\tau_{B,HH}(ATP)$, $\tau_{B,MWC}(ATP)$, and $\tau_{B,D}(ATP)$ are the mean burst durations given by the HH, the MWC, and the dimer (D) models, respectively, $F\ (= a/b)$ is the equilibrium constant for intraburst closures, c is the rate of closure of the slow gate in the absence of ATP, and m is a proportionality coefficient that determines how much the rate of slow gate closure is increased when ATP is bound. Note that the values of K_O and m vary with the different models, as indicated by the subscripts *HH*, *MWC*, and *D*.

Inspection of these equations reveals that, due to the imposed symmetry, they simply reflect the properties of the individual gating units in each model ($4GU_1$, $2GU_2$, $1GU_4$). Thus for the Hodgkin-Huxley model, there is one ATP-binding site per gating unit, for the dimer model there are two ATP-binding sites, and for the MWC model there are four ATP-binding sites. The coefficients 4, 1, and 2 in front of Eqs. 7–9 reflect the number of gating units in these models.

Eqs. 7–9 can be rearranged by multiplying each side of the equation by the mean burst duration in the absence of ATP (which is obtained by setting [ATP] to zero):

$$\frac{\tau_{B,HH}(0)}{\tau_{B,HH}([ATP])} = \frac{1 + m_{HH} * K_{O,HH} * [ATP]}{1 + K_{O,HH} * [ATP]} \quad (10)$$

$$\frac{\tau_{B,MWC}(0)}{\tau_{B,MWC}([ATP])} = \left(\frac{1 + m_{MWC} * K_{O,MWC} * [ATP]}{1 + K_{O,MWC} * [ATP]} \right)^4 \quad (11)$$

$$\frac{\tau_{B,D}(0)}{\tau_{B,D}([ATP])} = \left(\frac{1 + m_{D} * K_{O,D} * [ATP]}{1 + K_{O,D} * [ATP]} \right)^2. \quad (12)$$

In this form, the burst durations are expressed solely as a function of the ATP concentration and the ATP-dependent parameters K_O and m. Eqs. 10–12 thus allow comparison of the mean burst duration for channels with different open state energies (i.e., they remove the dependence on the rate constant c in Scheme 2). Since individual K_{ATP} channels (even of the same species) possess quite variable values of $\tau_B(0)$, plotting the ATP dependence of the mean burst durations averaged from several single-channel patches using Eqs. 10–12 instead of Eqs. 7–9 should substantially reduce error in the determination of K_O and m. Second, taking the intrinsic mean burst duration (i.e., that in the absence of ATP) as the average of that measured before and after ATP application should compensate for effects of K_{ATP} channel rundown.

For simplicity, we define the ratio of the mean burst duration in the absence of ATP to that in the presence of ATP, i.e., $\tau_B(0)/\tau_B([ATP])$ as the burst ratio (BR).

The Properties of Connected Tetramers for the Different Models

We next consider how the ATP dependence of BR varies with the gating models shown in Fig. 2 for the different tetrameric constructs. Eqs. 10–12 indicate that there are two ways in which a mutation may affect the ATP dependence of the burst ratio.

First, it may affect the affinity of ATP binding. Regardless of the gating mechanism, a reduction in ATP binding to the open state (K_O) would result in a decrease in the slope of the relationship between BR and ATP. A simultaneous reduction in K_O and K_C would also shift the macroscopic ATP dose–response curves to higher ATP concentrations. In the limiting case (where $K_O \approx 0$, $K_C \approx 0$), the channel will not bind ATP at all and gating will be unaffected by the ligand.

Second, a mutation may also affect the parameter m, which describes the increase in the rate of closure due to ATP binding to the open state. Regardless of the gating mechanism, a reduction in m would reduce the maximal extent of the decrease in the mean burst duration caused by ATP (Eqs. 10–12). If K_O and n in Scheme 2 are unaffected, it follows from the principle of microscopic reversibility that a decrease in m would simultaneously result in a decrease in K_C and in the ratio K_C/K_O (since $K_C = K_O * m/n$). A decrease in m will then have two effects on the ATP sensitivity of macroscopic K_{ATP} currents; it will shift the ATP dose–response curves to higher ATP concentrations (due to the decrease in K_C), and it will also increase the fraction of unblocked current at high ATP concentrations (via the increase in the K_O/K_C ratio). In principle, a change in m can be accompanied by a simultaneous change in n, which would either reduce (decrease in n) or enhance (increase in n) these effects. In the special case when $m \approx n$ and thus $t \approx 1$, the channel will still bind ATP but its gating will be completely unaffected by ligand binding.

Let us assume that the K185E mutation either (a) abolishes ATP binding to the open state ($K_O \approx 0$) or (b) abolishes the effect of ATP binding to the open state on channel closure ($m \approx 1$). For all three models, it is possible to show that the ATP dependence of the mean burst duration will be identical whether it is calculated assuming $K_O = 0$, or $m = 1$. The predictions for the different tetrameric constructs are shown in Fig. 3 (A–C).

It is clear that each model produces a distinct set of relationships between BR and ATP. In the case of the Hodgkin-Huxley model, the BR amplitude is simply proportional to the number of functional ATP-binding sites in the tetramer (Fig. 3 A). In contrast, for the MWC model, the BR amplitude decreases dramatically with the number of wild-type ATP-binding sites in the gating unit (Fig. 3 B). This is because the additive effect of ATP on the energy profile between open and interburst closed state(s) is translated into a multiplicative effect on burst duration. In the case of the dimer model, the BR amplitude is dramatically reduced when there is only one wild-type ATP-binding site per channel and the properties of channels with two functional ATP-binding sites depend on whether they lie within the same or different gating unit (Fig. 3 C).

Published June 30, 2008

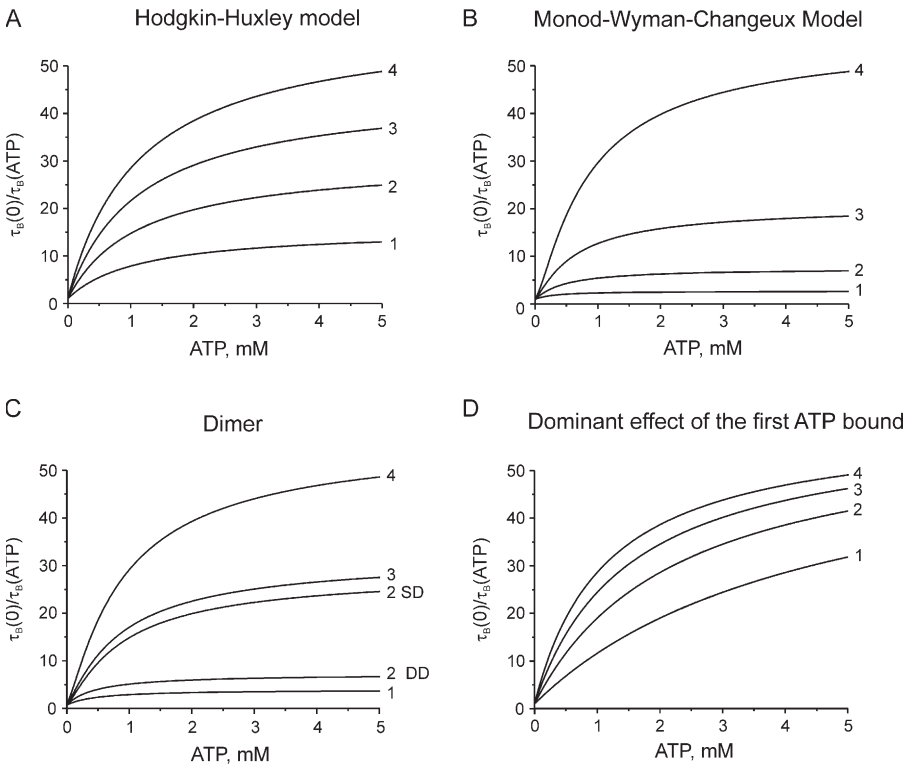

Figure 3. Predictions for the ATP dependence of the burst ratio for tetrameric constructs based on different models. Relationship between the burst ratio (BR) and ATP concentration for connected K_{ATP} tetramers containing between one and four WT ATP-binding sites for channels containing four (A), one (B) or two (C) gating units. These correspond to the HH, MWC, and D models respectively. D depicts the relationship when the first ATP bound has a dominant effect on channel closure. The number of WT ATP-binding sites is indicated to the right of each trace. 2 SD, tetrameric construct with 2WT ATP-binding sites located on the same dimer subunit; 2 DD, tetrameric construct with two WT ATP-binding sites each located on a different dimer subunit. The lines are fit assuming mutant ATP-binding sites are nonfunctional (i.e., $m = 1$ or $K_O = 0$). The lines are drawn using Eqs. 16–23 given in the Appendix. The K_O and m parameters for the wild-type subunits of each model were obtained by fitting the data for unconnected four WT K_{ATP} channels (Fig. S12 B, open circles).

In all models discussed so far we assumed independence of ATP binding and ATP-induced K_{ATP} channel closure. This may not be the case. One of the simplest possibilities that does not fulfill these two conditions is shown in Fig. 3 D. Because the Hill coefficient for K_{ATP} channel inhibition by ATP is close to 1, it is reasonable to assume that the first ATP bound to the channel may have a dominant effect on K_{ATP} channel closure. This can be modeled by assuming that only one ATP molecule can bind to the channel in the open conformation (top four states of the MWC model in Fig. 2). Using Eq. 6, the burst ratio in this case is given by:

$$\frac{\tau_B(0)}{\tau_B([ATP])} = \frac{1 + j * m * K_O * [ATP]}{1 + j * K_O * [ATP]}, \qquad (13)$$

where $j = 1...4$ is the number of functional ATP binding sites. In this case, a reduction in the number of wild-type ATP binding sites will have only a mild effect on the amplitude of BR (Fig. 3 D).

ATP-dependent Closure of K_{ATP} Channels Formed from Connected Tetramers Obeys the MWC Model

We next performed single-channel recordings for each of the concatenated tetramers shown in Fig. 1, to determine which ATP–BR relationship is found experimentally. Kir6.2 tetramers were coexpressed with SUR1 and all experiments were performed in Mg-free solution. We recorded single-channel activity from inside-out patches at three different ATP concentrations: 0.2, 1, and 5 mM. Fig. 4 shows representative single-channel records for each tetramer in the absence (top traces) and presence of 1 mM ATP (bottom traces). It is clear that as the number of wild-type ATP-binding sites in the tetramer is reduced, the ATP sensitivity of these channels is gradually impaired. This indicates that binding of a single ATP does not have a dominant effect.

Fig. 5 A gives the mean relationship between BR and ATP concentration for the different tetramers. Comparison of Fig. 5 A with Fig. 3 immediately suggests that the ATP dependence of BR resembles that predicted by the MWC mechanism. The properties of the MWC model can be seen more easily when the data are plotted on a log scale (Fig. 5 B). It then becomes clear that the burst duration of channels containing four mutant subunits (4M) still exhibits a mild ATP dependence. Interestingly, the K185E mutation does not appear to affect the affinity of ATP binding to the open state (K_O) as the ATP dependence of BR saturates at a similar ATP concentration to that of the wild-type channel for all channel species. Instead, it is clear that the mutation markedly alters the maximal amplitude of the relationship. Fitting the MWC model (Eq. 11) to the 4M data gave $K_{O,MWC} = 3.3 \pm 1.0$ mM^{-1} (i.e., the dissociation constant $K_d = 303 \pm 63$ μM) and $m_{MWC} = 1.13 \pm 0.01$.

From the log plot of the data it is also evident that the BR–ATP relationships for all tetramers are distributed at equal intervals and saturate in the same range of ATP concentrations. Thus, in accordance with the MWC model, the effects of ATP binding to both wild-type and mutated

Published June 30, 2008

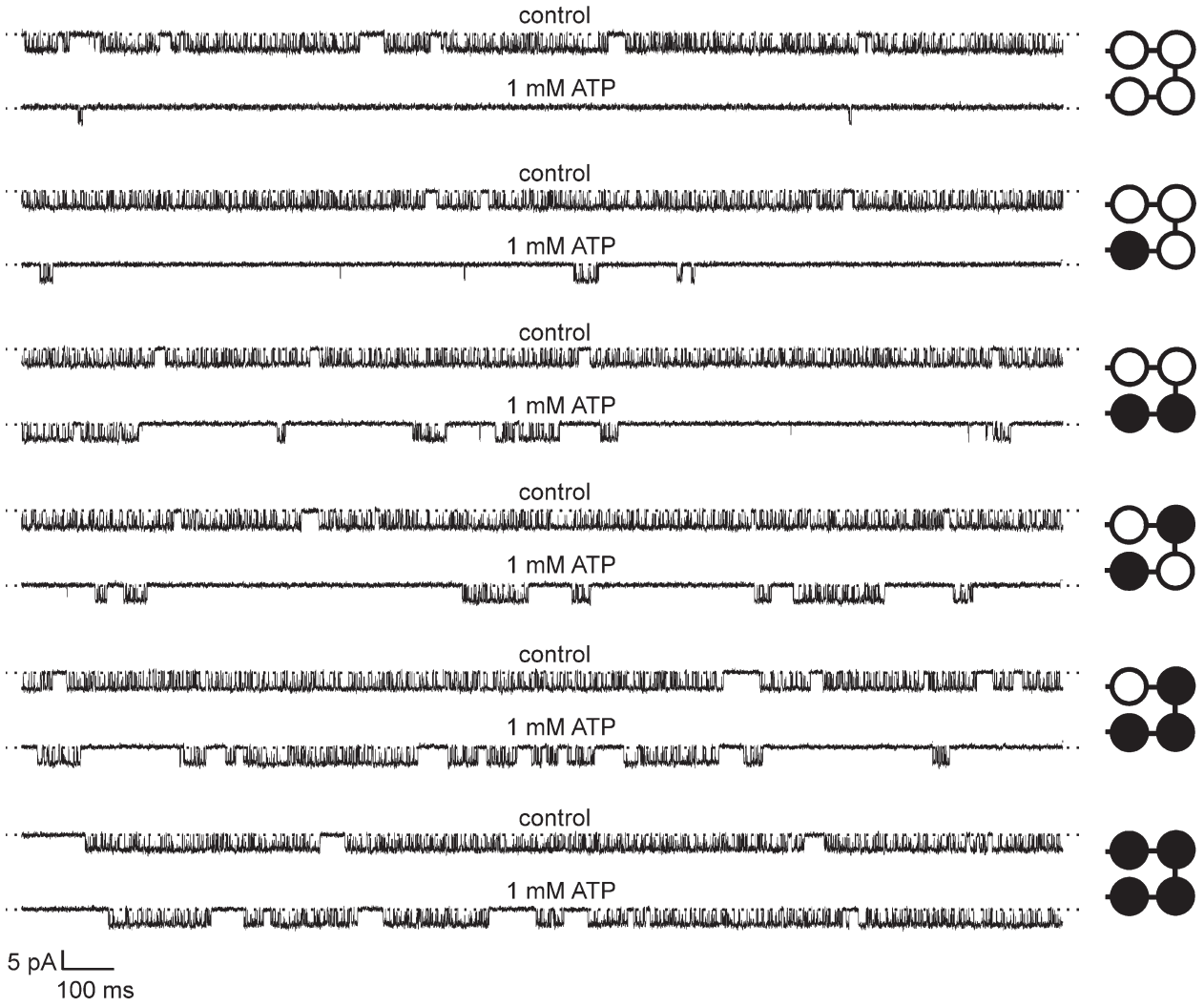

Figure 4. Single-channel recordings. Single-channel currents recorded from inside-out patches at −60 mV in the presence or absence of 1 mM ATP. The composition of each tetramer is shown schematically on the right. Open circles, WT subunits; filled circles, Kir6.2-K185E subunits. The dotted line indicates the zero current level.

ATP-binding sites appear to be additive. This allows all the data to be fit simultaneously with a single set of equations:

$$\frac{\tau_{B,i}(0)}{\tau_{B,i}([ATP])} = \left(\frac{1 + m_{WT} * K_{O,WT} * [ATP]}{1 + K_{O,WT} * [ATP]}\right)^{i} * \left(\frac{1 + m_{M} * K_{O,M} * [ATP]}{1 + K_{O,M} * [ATP]}\right)^{4-i}, \quad (14)$$

where $K_{O,WT}$ and $K_{O,M}$ are the binding constants for ATP to the open state for wild-type and mutant subunits, respectively; m_{WT} and m_M are the relative increases in the rate of the slow gate closure induced by ATP for wild-type and mutant subunits, respectively; and i is the number of wild-type subunits in the tetramer (i = 1–4). All the relationships could be well fit with the same set of parameters. The parameters for the 4M channel were assumed to be constant ($K_{O,M}$ = 3.3 mM^{-1}; m_M = 1.13) and were obtained from the fit to the 4M data. Those for the wild-type channel were derived from the global fit to all data obtained from channels containing at least one WT subunit. These were $K_{O,WT}$ = 3.1 ± 0.2 mM^{-1} (or the dissociation constant K_d = 320 ± 20 μM) and m_{WT} = 2.8 ± 0.1. These values were similar to those obtained by fitting the wild-type data alone (see Fig. 5 A). Thus, the K185E mutation appears to affect the burst duration predominantly by its action on the mechanism by which ATP binding to the open state is transduced into channel closure ($m_M \approx 1$).

Macroscopic Properties of K_{ATP} Channels Formed from Connected Kir6.2 Tetramers

We next determined the ATP sensitivity of all tetrameric constructs (Fig. 6 A). For these experiments we used macroscopic currents, as the ATP sensitivity can be measured more accurately and represents the mean of many channels. At this point, it is important to remember that

Published June 30, 2008

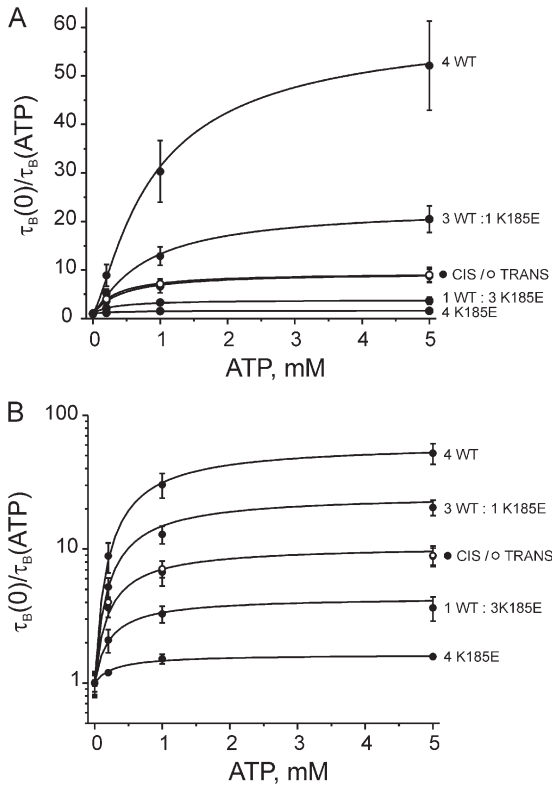

Figure 5. ATP dependence of burst ratio. Relationship between burst ratio and ATP concentration measured experimentally for connected K_{ATP} channel tetramers containing different numbers of wild-type and mutant subunits (as indicated to the right of each trace). Each data point is the average of three to five experiments. (A) Linear scale. The lines were generated by fitting Eq. 14 to the data for each tetramer separately. The best fit of Eq. 11 to the data for 4M channels gave values of $K_{O,M}$ = 3.3 mM^{-1} and m_M = 1.13, and these were used for the mutant subunits in all other fits. The best fit of Eq. 14 to K_{ATP} channels containing one to four WT subunits was obtained with the following values of $K_{O,WT}$ and m_{WT}: $K_{O,WT}$ = 5.0 mM^{-1}; m_{WT} = 2.7 (1WT:3M); $K_{O,WT}$ = 4.2 mM^{-1}; m_{WT} = 2.7 (2WT:2M cis); $K_{O,WT}$ = 5.3 mM^{-1}; m_{WT} = 2.7 (2WT:2M trans); $K_{O,WT}$ = 2.9 mM^{-1}; m_{WT} = 2.7 (3WT:1M); $K_{O,WT}$ = 3.1 mM^{-1}; m_{WT} = 2.8 (4WT). Log scale. The lines were generated with Eq. 14 using $K_{O,WT}$ = 3.1 mM^{-1}; m_{WT} = 2.8 for wild-type subunits and $K_{O,M}$ = 3.3mM^{-1}; m_M = 1.13 for K185E subunits (see text for details).

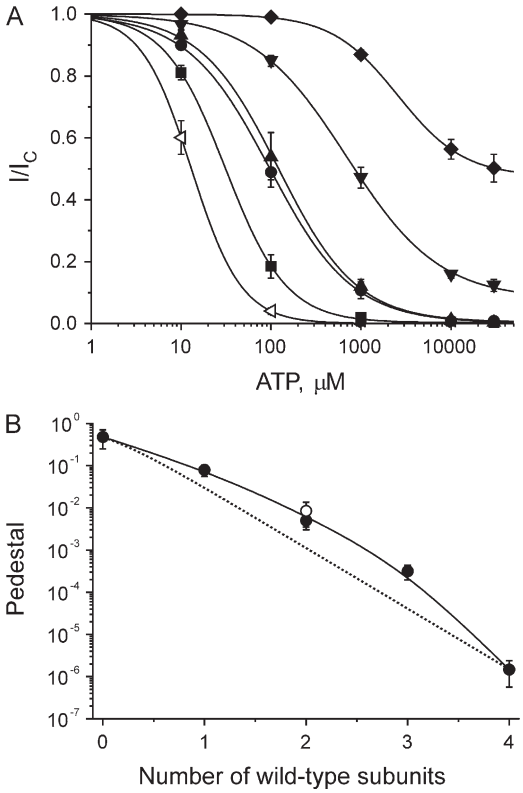

Figure 6. Macroscopic properties of connected tetramers. (A) Macroscopic dose–response curves for ATP inhibition of connected K_{ATP} channels containing different numbers of WT and K185E (M) subunits (◁, 4WT; ■, 3WT:1M; ●, 2WT:2M cis; ▲, 2WT:2M trans; ▼, 1WT:3M; ◆, 4M). n = 5 for all data. The lines are best fit of the data with Eq. 5 with IC_{50} = 2.6 mM, h = 1.18, P = 0.48 (4M); IC_{50} = 690 μM, h = 0.84, P = 0.08 (1WT:3M); IC_{50} = 14 μM, h = 1.36, P = 0 (4WT); IC_{50} = 31 μM, h = 1.27, P = 0 (3WT:1M); IC_{50} = 97 μM, h = 0.94, P = 0 (2WT:2M cis); IC_{50} = 122 μM, h = 0.98, P = 0 (2WT:2M trans). (B) Pedestal amplitude as a function of the number of wild-type subunits in the connected tetramer. Open circles, 2WT:2M trans; filled circles, all other species. The pedestal was estimated from data in A as (a) the fraction of unblocked current at 30mM ATP or (b) from fitting Eq. 5 to the data (4M, 1WT:3M). Solid line, spline function fit through the data; dotted line, prediction of the MWC model (Eq. 15) with P_O = 0.75, F = 0.21, E_0 = 0.12 (Table I) and values $K_{C,WT}/K_{O,WT}$ = 51 and $K_{C,M}/K_{O,M}$ = 1.9 obtained from the fit of homomeric wild-type and mutant tetramers.

the extent of ATP inhibition of the macroscopic currents will be determined not only by the effect of ATP on the open state (discussed above), but also by interaction of ATP with the long closed states of the channel. Thus this approach enables us to obtain (indirect) information on the long closed states.

The dose–response curve for ATP inhibition of connected 4M channels shows a substantial (~50%) fraction of unblocked current (p) at high ATP concentrations (Fig. 6 A). This is predicted for a mutation that does not abolish ATP binding to the open state, but rather causes a defect in the mechanism by which ATP binding is transduced into channel closure (m in Scheme 2), and thus decreases the K_C/K_O ratio (see above). The fact that the IC_{50} for ATP inhibition of macroscopic currents through 4M channels was also increased indicates that the K185E mutation also reduces the affinity of ATP binding to the long closed states (K_C).

In comparison with other concatenated tetramers, connected 4M channels exhibited more pronounced rundown; consequently, the values of IC_{50} and p for ATP inhibition of these species decreased noticeably with time after patch excision. Thus, the estimates of IC_{50} and p from single-channel experiments, conducted over a long period of time (up to 20 min) were smaller than those from macroscopic experiments, obtained shortly after patch excision (see Fig. S11, available at http://www.jgp.org/cgi/content/full/jgp.200709874/DC1).

Published June 30, 2008

TABLE I

Single-Channel and Macroscopic Parameters of Homomeric Wild-Type K_{ATP} Channels

Parameter	Obtained from	Connected tetramers	Unconnected tetramers
IC_{50}	macroscopic data	14.5 ± 2.5 μM	8.4 ± 2.9 μM
h	macroscopic data	1.42 ± 0.07	1.22 ± 0.16
P_O	single-channel data	0.75 ± 0.04	0.33 ± 0.10
$\tau_B(0)$	single-channel data	127 ± 18 ms	20.7 ± 6.0 ms
a	$\tau_O(0)$, $\tau_B(0)$	0.59 ± 0.02 ms^{-1}	0.54 ± 0.07 ms^{-1}
b	$\tau_F(0)$	2.8 ± 0.1 ms^{-1}	2.7 ± 0.3 ms^{-1}
c	$\tau_O(0)$, $\tau_B(0)$	0.009 ± 0.001 ms^{-1}	0.06 ± 0.02 ms^{-1}
F	a and b	0.21 ± 0.03	0.20 ± 0.05
E_0	P_O	0.12 ± 0.02	1.83 ± 1.01
$K_{O,WT}$	$\tau_B(0)/\tau_B([ATP])$	3.1 ± 0.2 mM^{-1}	3.2 ± 0.2 mM^{-1}
$K_{O,WT}$	$\tau_O([ATP])$	3.8 ± 0.9 mM^{-1}	3.2 ± 0.2 mM^{-1}
m_{WT}	$\tau_B(0)/\tau_B([ATP])$	2.8 ± 0.1	2.7 ± 0.1
m_{WT}	$\tau_O([ATP])$	2.4 ± 0.1	2.5 ± 0.1

n = 5 for macroscopic data; n = 10 for single-channel data. Values of $K_{O,WT}$ and m_{WT} were obtained by fitting the MWC model (Eq. 11 for burst ratios and Eq. S4 for open times) to the mean values obtained from three to five experiments. All other parameters were calculated from 10 experiments.

The fraction of unblockable current was decreased, but not abolished, for channels containing one wild-type ATP-binding site. The fact that ATP inhibition of cis and trans 2WT:2M species by ATP was almost identical suggests that ATP-dependent gating of connected tetramers does not involve dimeric transitions.

The MWC model assumes transitions only occur between two classes of states (Monod et al., 1965). If ATP binding to single subunit (in the tetramer) is independent of binding to the other subunits for all interburst closed states, then it is possible to lump the interburst closed states together (i.e., as C_s). The gating between the open and the lumped closed state (C_s) can then be described with MWC model. This model can then be used to describe the macroscopic ATP dose–response curve of the K_{ATP} channel, as in Fig. 2 B.

We tested the possibility that the MWC model can be used to describe the measured macroscopic ATP dose–response curve. We fitted the values of the pedestal, p_i, which we define as the fraction of unblocked current at saturating ATP concentration for channels with i WT subunits. Fig. 6 B plots the pedestal, for the data shown in Fig. 6 A, as a function of the number of wild-type subunits. For the MWC model, p_i is given by

$$p_i = \frac{1}{P_O * (1+F) + P_O * E_0 * \left(\frac{K_{C,WT}}{K_{O,WT}}\right)^i * \left(\frac{K_{C,M}}{K_{O,M}}\right)^{4-i}}, \quad (15)$$

where $K_{C,WT}$ and $K_{C,M}$ are the binding constants for ATP to the lumped interburst closed state (C_s) for wild-type and mutant subunits, respectively; $K_{O,WT}$ and $K_{O,M}$ are the binding constants for ATP to the open state for wild-type and mutant subunits, respectively; $E_0 = c/d$ is the equilibrium gating constant for transitions between the open and the lumped closed state (see Schemes 1 and 2), P_O is the intrinsic open probability and i is the number of wild-type subunits in the tetramer.

All tetrameric constructs had similar initial values of intrinsic P_O: 0.75 ± 0.04, n = 10 (4WT); 0.75 ± 0.02, n = 11 (3WT1M); 0.75 ± 0.02, n = 11 (cis); 0.74 ± 0.04, n = 10 (trans); 0.74 ± 0.03, n = 8 (3M1WT); 0.71 ± 0.05, n = 7 (4M). Using the values of P_O, F, and E_0 given in Table I, it is possible to calculate the ratios $K_{C,WT}/K_{O,WT}$ and $K_{C,M}/K_{O,M}$ from the corresponding values of p_4 and p_0 using Eq. 15. These ratios can be used to obtain values of p for the MWC model (dotted line in Fig. 6 B). As Fig. 6 B shows, the data deviate from the model, suggesting that the assumption that ATP binding to one subunit is independent of that to the other subunits is not correct for at least some of the interburst closed states. Thus the data suggest that while the MWC model can be applied to the transitions between the open state and one or more of the interburst closed states, it cannot be applied to all of the transitions between the different interburst closed states.

It is of course possible that this effect is specific to the K185E mutation and is not observed for other mutations in the ATP-binding site. The deviations from the MWC model observed at high ATP concentrations could result from an effect of the K185E mutation on intersubunit interactions between ATP-binding sites when the channel is closed. We found no obvious effect on the intrinsic open probability of connected homomeric WT channels (P_O = 0.75 ± 0.04, n = 10) and connected homomeric K185E tetramers (P_O = 0.71± 0.05, n = 7). However, this does not mean that the mutation cannot somehow alter the distribution of interburst closed states. Unfortunately, this is very difficult to measure accurately.

Published June 30, 2008

Comparison of Properties of K_{ATP} Channels Formed from Connected and Separate Kir6.2 Subunits

Finally, in order to assess the physiological relevance of the results we obtained on connected tetramers, we examined the single-channel properties of unconnected tetramers. Full details are given in the online supplementary material (available at http://www.jgp.org/cgi/content/full/jgp.200709874/DC1); here we summarize only the major results.

Effects on Open States

The values of K_O and m obtained from the best fit of the BR data for separated 4WT channels with the MWC model (Eq. 11) were $K_{O,WT}$ = 3.25 mM^{-1} (K_d = 308 μM) and m_{WT} = 2.7 (Table I). These values are very similar to those for the connected 4WT channel (K_d = 320 μM, m_{WT} = 2.8). Thus we conclude that the linkers introduced between Kir6.2 subunits in connected tetramers do not substantially alter ATP binding to the open state (K_O) or the transduction parameter m.

Similar values for K_O and m were also obtained from fitting the ATP dependence of the mean open times obtained for both connected and unconnected 4WT K_{ATP} channels (Table I; Fig. S13 C). These results provide further support for the idea that ATP reduces the burst duration via interaction with the open state of the channel (Li et al., 2002). They also confirm that ATP exerts only a mild effect on the intraburst transitions (thus validating the use of Scheme 2) and indicate that errors associated with the methods employed for measuring burst durations and open times were small.

To examine the properties of unconnected K_{ATP} channels containing various numbers of mutant subunits, we analyzed single-channel records from patches pulled from oocytes injected with different ratios of wild-type and mutant Kir6.2 mRNAs (Fig. S12 A). In single-channel patches, it was possible to identify channels with kinetic signatures that resembled those observed for connected tetramers with different numbers of WT and M subunits. The BR-ATP relationship for these channels was similar to that of the corresponding connected tetramers (Fig. S12 B). We therefore conclude that in unconnected mixed WT:M tetramers, as in their connected counterparts, ATP binding to Kir6.2 is also likely to be independent.

The intrinsic P_O of connected 4WT K_{ATP} channels was ~2.3-fold higher than that of unconnected 4WT channels (Table I). The mean burst duration was also increased (approximately sixfold, Table I). Calculation of the intrinsic rate constants *a*, *b*, and *c* from data obtained in the absence of ATP indicated that these effects are caused by a decrease in the rate constant *c* in the connected tetramer (Table I). Such a shift in the gating equilibrium toward the open state is expected to indirectly reduce the ATP sensitivity of the K_{ATP} channel (Trapp et al., 1998). As anticipated, connected 4WT tetramers had a slightly reduced ATP sensitivity: the IC_{50} increased from 8.4 to 14.5 μM (Table I). This small increase in IC_{50} can be fully accounted for by the sixfold increase in the mean burst duration (Trapp et al., 1998).

Taken together, these results indicate that connected tetramers provide a good model for studying the interaction of ATP with the open state of the K_{ATP} channel. Although the increase in intrinsic P_O altered the ATP sensitivity, it also substantially stabilized channel activity in excised patches, making it particularly suitable for analysis of single-channel kinetics.

Effects on Interburst Closed States

The high intrinsic P_O of concatenated tetramers implies that in comparison with unconnected tetramers, the interaction of ATP with the interburst closed states of the channel will be substantially reduced. It would therefore be expected that concatenated tetramers would be less inhibited by ATP than unconnected tetramers at nucleotide concentrations where ATP binding saturates (i.e., in Eq. 15 for the MWC model, reduced E_0 values would increase p_i). Interestingly, we observed the opposite effect; at 10 mM ATP, the fraction of current that remained unblocked was $1.7 \pm 0.7*10^{-6}$ (n = 6) and $1.0 \pm 0.6*10^{-5}$ (n = 6) for connected and unconnected K_{ATP} channels composed of four wild-type subunits. Thus, in addition to increasing the stability of the open state, linking Kir6.2 subunits also enhanced the efficiency of K_{ATP} channel inhibition by ATP. Since ATP-dependent closure from the open state in connected tetramers is not substantially altered, this effect must involve the stabilization of long closed states of the channel by the nucleotide. Thus, the effect of ATP on the interburst duration of connected tetramers does not quantitatively match that of the unconnected channel.

DISCUSSION

In this paper, we show that the ATP dependence of the mean burst duration of connected tetramers can be used to determine the mechanism by which ATP induces closing of the K_{ATP} channel. Although experimentally laborious, this method can be easily extended for other types of ligand-gated multimeric ion channels.

We considered the possibility that the subunits within a concatenated tetramer do not assemble into the same tetrameric channel, as previously suggested for connected dimers of Shaker K^+ channels (McCormack et al., 1992). However, this did not seem to be the case. Each of the different tetrameric channels we constructed had very different single-channel properties. Expression of a single tetrameric species gave rise to single channels with similar properties; we never observed channels with properties corresponding to more than one type of channel. It is possible that the presence of SUR1, which surrounds the Kir6.2 tetramer (Mikhailov et al., 2005), may act as a chaperone, or simply as a physical obstruction,

Published June 30, 2008

and prevent aberrant associations between subunits from two different concatenated tetramers.

Effects of ATP on the Open State

We show (for the first time) that the decrease in the burst and open time duration of the K_{ATP} channel produced by ATP saturates at high ATP concentration. This is indicative of the existence of ATP bound-open states in the wild-type channel. Analysis of burst and open times can be thus expanded to include effects of all four ATP molecules on channel closure. In contrast, previous studies considered the effect of only one ATP molecule on channel closure because they assumed a linear relationship between $1/\tau_O$ and [ATP] (Davies et al., 1992; Li et al., 2002).

Our results demonstrate that the ATP-dependent decrease in mean open and burst durations can be described by the MWC mechanism. Together with the data obtained by Drain et al. (2004), it can thus be concluded that Kir6.2 subunits (either liganded or unliganded) exert an additive effect on the energy of the open state of the channel. Furthermore, our results show that when the channel is open, ATP binds to a single ATP-binding site with a K_d of ~300 μM (as the channel has four ATP-binding sites, the overall K_d for binding to the open state is ~75 μM). This means that in the intact cell, where ATP ranges from 1 to 10 mM, an open channel will have ATP bound to Kir6.2 for most of the time.

The MWC model is inherently easier to reconcile with the structure of the K_{ATP} channel than are the other two models tested. Let us consider that each gating unit represents the cytosolic domain of a single Kir6.2 subunit. In the HH model, the cytosolic domain of an individual Kir6.2 subunit undergoes a conformational change on ATP binding that does not influence other subunits. In the MWC model, the four cytosolic domains function as a single unit, and ATP binding to a single subunit produces a global conformational change in all four cytosolic domains that leads to pore closure. This seems reasonable, given that residues in two adjacent subunits contribute to a single ATP-binding site in a molecular model of Kir6.2 (Antcliff et al., 2005).

Since we restricted our analysis to the mean burst durations, it is possible that more complex concerted models than the MWC model will be required to describe the ATP-dependent closing reaction fully. However, our data suggest that any such model will also have to be concerted. Furthermore, in order to produce the exponential dependence of burst duration on the number of wild-type subunits (Figs. 2 and 5), it should also satisfy the criterion that ATP binding at one subunit is independent of other subunits.

Effects of K185E Mutation on ATP Binding

Residue K185 plays crucial a key role in ATP binding to Kir6.2. Mutation of K185 has a marked effect on ATP block of channel activity (Reimann et al., 1999; John et al., 2003; Ribalet et al., 2003; Wang et al., 2007), and binding of labeled ATP to Kir6.2 is reduced when K185 is mutated (Tanabe et al., 2000). Molecular dynamic simulations of ATP binding to a homology model of Kir6.2 suggest that the strongest interaction of ATP with Kir6.2 is via the side chain of K185 (Haider et al., 2005b). Our results show that the K185E mutation does not alter the affinity of ATP binding to the open state but instead impairs the conformational change induced on ATP binding that leads to channel closure. The affinity of ATP binding to the closed state of the channel is also impaired. Taken together, the data are consistent with a model in which residue 185 may not be accessible to ATP in the open state, but where the closure of the channel leads to a conformational change that facilitates entry of ATP into its binding site, thereby providing access to residue 185. The lack of effect of replacing lysine with glutamate on ATP binding to the open state also raises the possibility that residue 185 does not interact directly with ATP as implied by molecular modeling (Antcliff et al., 2005), or that it only interacts in the closed state.

Conclusions

Our results demonstrate that it is important to consider the interaction of ATP with the open state of the channel for both a qualitative and a quantitative understanding of ATP inhibition. We have previously used this interaction to quantify a gating defect caused by the C166S mutation (Trapp et al. 1998). In this study, we show how the ATP-dependent closing rate can be also used to measure ATP binding and to quantify the mechanism by which ATP binding is transduced into channel closure. The latter is of particular interest as this mechanism is poorly understood. The fact that the ATP dependence of the mean open and burst durations can be described by a simple MWC model is useful for the analysis of the molecular mechanism of K_{ATP} channel mutations, such as those that cause neonatal diabetes (Ashcroft, 2005; Hattersley and Ashcroft, 2005). In the future, it will be necessary to develop more complex kinetic models in order to describe the gating of K_{ATP} channels more completely.

APPENDIX

Modeling of the ATP Dependence of the BR of Unconnected Wild-Type K_{ATP} Channels for the Different Types of Models (Fig. 3)

Fig. 2 A and Fig. 3 A. The Hodgkin-Huxley model ($4GU_1$). The lines were drawn to

$$\frac{\tau_{B,HH}(0)}{\tau_{B,HH}([ATP])} = 1 + \frac{j*(m_{HH}-1)*K_{O,HH}*[ATP]}{4*(1+K_{O,HH}*[ATP])}, \quad (16)$$

where $j = 1...4$ is the number of wild-type subunits in the tetramer, $K_{O,HH} = 0.88\ \mathrm{mM}^{-1}$, and $m_{HH} = 60$.

Published June 30, 2008

Fig. 2 B and Fig. 3 B. The Monod-Wyman-Changeux model (GU_4). The lines were drawn to

$$\frac{\tau_{B,MWC}(0)}{\tau_{B,MWC}([ATP])} = \left(\frac{1 + m_{MWC} * K_{O,MWC} * [ATP]}{1 + K_{O,MWC} * [ATP]}\right)^{j}, \quad (17)$$

where $j = 1..4$ is the number of wild-type subunits in the tetramer, $K_{O,MWC} = 3.2\ \mathrm{mM}^{-1}$, and $m_{MWC} = 2.7$.

Fig. 2 C and Fig. 3 C. The dimer model ($2GU_2$). The lines were drawn according to the following equations with $K_{O,D} = 2.1\ \mathrm{mM}^{-1}$ and $m_D = 7.3$:

$$\frac{\tau_{B,D}(0)}{\tau_{B,D}([ATP])} = \left(\frac{1 + m_D * K_{O,D} * [ATP]}{1 + K_{O,D} * [ATP]}\right)^{2} \quad (18)$$

$$\frac{\tau_{B,D}(0)}{\tau_{B,D}([ATP])} = \frac{(1 + m_D * K_{O,D} * [ATP]) * \left(1 + \frac{(1 + m_D) * K_{O,D} * [ATP]}{2}\right)}{(1 + K_{O,D} * [ATP])^2} \quad (19)$$

$$\frac{\tau_{B,D}(0)}{\tau_{B,D}([ATP])} = \frac{1 + m_D * K_{O,D} * [ATP]}{1 + K_{O,D} * [ATP]} \quad (20)$$

$$\frac{\tau_{B,D}(0)}{\tau_{B,D}([ATP])} = \frac{\left(1 + K_{O,D} * [ATP] * \left(1 + m_D + K_{O,D} * [ATP]\frac{1 + m_D^{\,2}}{2}\right)\right)}{(1 + K_{O,D} * [ATP])^2} \quad (21)$$

$$\frac{\tau_{B,D}(0)}{\tau_{B,D}([ATP])} = \frac{1 + \frac{1 + m_D}{2} K_{O,D} * [ATP]}{1 + K_{O,D} * [ATP]} \quad (22)$$

for channels with 4 (Eq. 19), 3 (Eq. 19), 2DD (Eq. 20), 2SD (Eq. 21), and 1 (Eq. 22) functional ATP-binding site(s).

Fig. 2 D. The lines were drawn to

$$\frac{\tau_{B,DOM}(0)}{\tau_{B,DOM}([ATP])} = \frac{1 + j * m_{DOM} * K_{O,DOM} * [ATP]}{1 + j * K_{O,DOM} * [ATP]}, \quad (23)$$

where $j = 1 \ldots 4$ is the number of functional ATP-binding sites, $K_{O,DOM} = 0.22\ \mathrm{mM}^{-1}$, and $m_{DOM} = 60$.

We thank Chris Miller (Brandeis University, Waltham, MA) for constructive criticism and advice on an earlier version of the manuscript. We also thank the referees for valuable insights.

We thank the European Union (BIOSIM) and the Wellcome Trust for support. T. Craig is an OXION Training Fellow. F.M. Ashcroft is a Royal Society Research Professor.

Olaf S. Andersen served as editor.

Submitted: 16 August 2007
Accepted: 30 May 2008

REFERENCES

Abraham, M.R., V.A. Selivanov, D.M. Hodgson, D. Pucar, L.V. Zingman, B. Wieringa, P.P. Dzeja, A.E. Alekseev, and A. Terzic. 2002. Coupling of cell energetics with membrane metabolic sensing. Integrative signalling through creatine kinase phosphotransfer disrupted by M-CK gene knock-out. *J. Biol. Chem.* 277:24427–24434.

Alekseev, A.E., P.A. Brady, and A. Terzic. 1998. Ligand-insensitive state of cardiac ATP-sensitive K^+ channels -basis for channel opening. *J. Gen. Physiol.* 111:381–394.

Antcliff, J.F., S. Haider, P. Proks, M.S. Sansom, and F.M. Ashcroft. 2005. Functional analysis of a structural model of the ATP-binding site of the K_{ATP} channel Kir6.2 subunit. *EMBO J.* 24:229–239.

Ashcroft, F.M. 2005. ATP-sensitive potassium channelopathies: focus on insulin secretion. *J. Clin. Invest.* 115:2047–2058.

Ashcroft, F.M., D.E. Harrison, and S.J. Ashcroft. 1984. Glucose induces closure of single potassium channels in isolated rat pancreatic β-cells. *Nature.* 312:446–448.

Clement, J.P. IV, K. Kunjilwar, G. Gonzalez, M. Schwanstecher, U. Panten, L. Aguilar-Bryan, and J. Bryan. 1997. Association and stoichiometry of K_{ATP} channel subunits. *Neuron.* 18:827–838.

Colquhoun, D. 1998. Binding, gating, affinity and efficacy: the interpretation of structure-activity relationships for agonists and of the effects of mutating receptors. *Br. J. Pharmacol.* 125:924–947.

Colquhoun, D., and A.G. Hawkes. 1982. On the stochastic properties of bursts of single ion channel openings and of clusters of bursts. *Philos. Trans. R. Soc. Lond. B Biol. Sci.* 300:1–59.

Davies, N.W., N.B. Standen, and P.R. Stanfield. 1992. The effect of intracellular pH on ATP-dependent potassium channels of frog skeletal muscle. *J. Physiol.* 445:549–568.

Drain, P., L. Li, and J. Wang. 1998. K_{ATP} channel inhibition by ATP requires distinct functional domains of the cytoplasmic C terminus of the pore-forming subunit. *Proc. Natl. Acad. Sci. USA.* 95:13953–13958.

Drain, P., X. Geng, and L. Li. 2004. Concerted gating mechanism underlying K_{ATP} channel inhibition by ATP. *Biophys. J.* 86:2101–2112.

Enkvetchakul, D., G. Loussouarn, E. Makhina, S.L. Shyng, and C.G. Nichols. 2000. The kinetic and physical basis of K_{ATP} channel gating: toward a unified molecular understanding. *Biophys. J.* 78:2334–2348.

Enkvetchakul, D., G. Loussouarn, E. Makhina, and C.G. Nichols. 2001. ATP interaction with the open state of the K_{ATP} channel. *Biophys. J.* 80:719–728.

Fan, Z., and J.C. Makielski. 1999. Phosphoinositides decrease ATP sensitivity of the cardiac ATP-sensitive K^+ channel. A molecular probe for the mechanism of ATP-sensitive inhibition. *J. Gen. Physiol.* 114:251–269.

Fang, K., L. Csanady, and K.W. Chan. 2006. The N-terminal transmembrane domain (TMD0) and a cytosolic linker (L0) of sulphonylurea receptor define the unique intrinsic gating of K_{ATP} channels. *J. Physiol.* 576:379–389.

Gillis, K.D., W.M. Gee, A. Hammoud, M.L. McDaniel, L.C. Falke, and S. Misler. 1989. Effects of sulfonamides on a metabolite-regulated ATP_i-sensitive K^+ channel in rat pancreatic B-cells. *Am. J. Physiol.* 257:C1119–C1127.

Gong, B., T. Miki, S. Seino, and J.M. Renaud. 2000. A K_{ATP} channel deficiency affects resting tension, not contractile force, during fatigue in skeletal muscle. *Am. J. Physiol. Cell Physiol.* 279:C1351–C1358.

Gribble, F.M., P. Proks, B.E. Corkey, and F.M. Ashcroft. 1998. Mechanism of cloned ATP-sensitive potassium channel activation by oleoyl-CoA. *J. Biol. Chem.* 273:26383–26387.

Haider, S., A. Grottesi, B.A. Hall, F.M. Ashcroft, and M.S. Sansom. 2005a. Conformational dynamics of the ligand-binding domain of inward rectifier K channels as revealed by molecular dynamics simulations: toward an understanding of Kir channel gating. *Biophys. J.* 88:3310–3320.

Haider, S., J.F. Antcliff, P. Proks, M.S. Sansom, and F.M. Ashcroft. 2005b. Focus on Kir6.2: a key component of the ATP-sensitive potassium channel. *J. Mol. Cell. Cardiol.* 38:927–936.

Hattersley, A.T., and F.M. Ashcroft. 2005. Activating mutations in Kir6.2 and neonatal diabetes: new clinical syndromes, new scientific insights, and new therapy. *Diabetes.* 54:2503–2513.

Hernandez-Sanchez, C., A.S. Basile, I. Fedorova, H. Arima, B. Stannard, A.M. Fernandez, Y. Ito, and D. LeRoith. 2001. Mice transgenically overexpressing sulfonylurea receptor 1 in forebrain resist seizure induction and excitotoxic neuron death. *Proc. Natl. Acad. Sci. USA.* 98:3549–3554.

Hodgkin, A.L., and A.F. Huxley. 1952. A quantitative description of membrane current and its application to conduction and excitation in nerve. *J. Physiol.* 117:500–544.

Inagaki, N., T. Gonoi, J.P. Clement IV, N. Namba, J. Inazawa, G. Gonzalez, L. Aguilar-Bryan, S. Seino, and J. Bryan. 1995. Reconstitution of IK_{ATP}: an inward rectifier subunit plus the sulfonylurea receptor. *Science.* 270:1166–1170.

John, S.A., J.N. Weiss, L.H. Xie, and B. Ribalet. 2003. Molecular mechanism for ATP-dependent closure of the K^+ channel Kir6.2. *J. Physiol.* 552:23–34.

Kane, G.C., X.K. Liu, S. Yamada, T.M. Olson, and A. Terzic. 2005. Cardiac K_{ATP} channels in health and disease. *J. Mol. Cell. Cardiol.* 38:937–943.

Li, L., X. Geng, and P. Drain. 2002. Open state destabilization by ATP occupancy is mechanism speeding burst exit underlying K_{ATP} channel inhibition by ATP. *J. Gen. Physiol.* 119:105–116.

Liss, B., R. Bruns, and J. Roeper. 1999. Alternative sulfonylurea receptor expression defines metabolic sensitivity of K_{ATP} channels in dopaminergic midbrain neurons. *EMBO J.* 18:833–846.

Liss, B., O. Haeckel, J. Wildmann, T. Miki, S. Seino, and J. Roeper. 2005. K_{ATP} channels promote the differential degeneration of dopaminergic midbrain neurons. *Nat. Neurosci.* 8:1742–1751.

Liu, X.K., S. Yamada, G.C. Kane, A.E. Alekseev, D.M. Hodgson, F. O'Cochlain, A. Jahangir, T. Miki, S. Seino, and A. Terzic. 2004. Genetic disruption of Kir6.2, the pore-forming subunit of ATP-sensitive K^+ channel, predisposes to catecholamine-induced ventricular dysrhythmia. *Diabetes.* 53(Suppl. 3):S165–S168.

MacDonald, P.E., Y.Z. De Marinis, R. Ramracheya, A. Salehi, X. Ma, P.R. Johnson, R. Cox, L. Eliasson, and P. Rorsman. 2007. A K_{ATP} channel-dependent pathway within alpha cells regulates glucagon release from both rodent and human islets of Langerhans. *PLoS Biol.* 5:e143.

Magleby, K.L., and B.S. Pallotta. 1983. Burst kinetics of single calcium-activated potassium channels in cultured rat muscle. *J. Physiol.* 344:605–623.

Markworth, E., C. Schwanstecher, and M. Schwanstecher. 2000. ATP^{4-} mediates closure of pancreatic β-cell ATP-sensitive potassium channels by interaction with 1 of 4 identical sites. *Diabetes.* 49:1413–1418.

McCormack, K., L. Lin, L.E. Iverson, M.A. Tanouye, and F.J. Sigworth. 1992. Tandem linkage of Shaker K^+ channel subunits does not ensure the stoichiometry of expressed channels. *Biophys. J.* 63:1406–1411.

Mikhailov, M.V., J.D. Campbell, H. de Wet, K. Shimomura, B. Zadek, R.F. Collins, M.S. Sansom, R.C. Ford, and F.M. Ashcroft. 2005. 3-D structural and functional characterization of the purified K_{ATP} channel complex Kir6.2-SUR1. *EMBO J.* 24:4166–4175.

Miki, T., B. Liss, K. Minami, T. Shiuchi, A. Saraya, Y. Kashima, M. Horiuchi, F. Ashcroft, Y. Minokoshi, J. Roeper, and S. Seino. 2001. ATP-sensitive K^+ channels in the hypothalamus are essential for the maintenance of glucose homeostasis. *Nat. Neurosci.* 4:507–512.

Miki, T., M. Suzuki, T. Shibasaki, H. Uemura, T. Sato, K. Yamaguchi, H. Koseki, T. Iwanaga, H. Nakaya, and S. Seino. 2002. Mouse model of Prinzmetal angina by disruption of the inward rectifier Kir6.1. *Nat. Med.* 8:466–472.

Monod, J., J. Wyman, and J.P. Changeux. 1965. On the nature of allosteric transitions: a plausible model. *J. Mol. Biol.* 12:88–118.

Nichols, C.G., W.J. Lederer, and M.B. Cannell. 1991. ATP dependence of K_{ATP} channel kinetics in isolated membrane patches from rat ventricle. *Biophys. J.* 60:1164–1177.

Nichols, C.G., S.L. Shyng, A. Nestorowicz, and B. Glaser, J.P. Clement IV, G. Gonzalez, L. Aguilar-Bryan, M.A. Permutt, and J. Bryan. 1996. Adenosine diphosphate as an intracellular regulator of insulin secretion. *Science.* 272:1785–1787.

Reimann, F., and F.M. Gribble. 2002. Glucose-sensing in glucagon-like peptide-1-secreting cells. *Diabetes.* 51:2757–2763.

Reimann, F., T.J. Ryder, S.J. Tucker, and F.M. Ashcroft. 1999. The role of lysine 185 in the Kir6.2 subunit of the ATP-sensitive channel in channel inhibition by ATP. *J. Physiol.* 520(Pt 3):661–669.

Ribalet, B., S.A. John, and J.N. Weiss. 2003. Molecular basis for Kir6.2 channel inhibition by adenine nucleotides. *Biophys. J.* 84:266–276.

Sakura, H., C. Ammala, P.A. Smith, F.M. Gribble, and F.M. Ashcroft. 1995. Cloning and functional expression of the cDNA encoding a novel ATP-sensitive potassium channel subunit expressed in pancreatic β-cells, brain, heart and skeletal muscle. *FEBS Lett.* 377:338–344.

Selivanov, V.A., A.E. Alekseev, D.M. Hodgson, P.P. Dzeja, and A. Terzic. 2004. Nucleotide-gated K_{ATP} channels integrated with creatine and adenylate kinases: amplification, tuning and sensing of energetic signals in the compartmentalized cellular environment. *Mol. Cell. Biochem.* 256-257:243–256.

Shelley, C., and D. Colquhoun. 2005. A human congenital myasthenia-causing mutation (epsilon L78P) of the muscle nicotinic acetylcholine receptor with unusual single channel properties. *J. Physiol.* 564:377–396.

Tanabe, K., S.J. Tucker, F.M. Ashcroft, P. Proks, N. Kioka, T. Amachi, and K. Ueda. 2000. Direct photoaffinity labeling of Kir6.2 by [g-32P]ATP-[g]4-azidoanilide. *Biochem. Biophys. Res. Commun.* 272:316–319.

Trapp, S., P. Proks, S.J. Tucker, and F.M. Ashcroft. 1998. Molecular analysis of ATP-sensitive K channel gating and implications for channel inhibition by ATP. *J. Gen. Physiol.* 112:333–349.

Trapp, S., S. Haider, P. Jones, M.S. Sansom, and F.M. Ashcroft. 2003. Identification of residues contributing to the ATP binding site of Kir6.2. *EMBO J.* 22:2903–2912.

Tucker, S.J., F.M. Gribble, C. Zhao, S. Trapp, and F.M. Ashcroft. 1997. Truncation of Kir6.2 produces ATP-sensitive K^+ channels in the absence of the sulphonylurea receptor. *Nature.* 387:179–183.

Tucker, S.J., F.M. Gribble, P. Proks, S. Trapp, T.J. Ryder, T. Haug, F. Reimann, and F.M. Ashcroft. 1998. Molecular determinants of K_{ATP} channel inhibition by ATP. *EMBO J.* 17:3290–3296.

Wang, R., X. Zhang, N. Cui, J. Wu, H. Piao, X. Wang, J. Su, and C. Jiang. 2007. Subunit-stoichiometric evidence for Kir6.2 channel gating, ATP binding, and binding-gating coupling. *Mol. Pharmacol.* 71:1646–1656.

Yamada, K., J.J. Ji, H. Yuan, T. Miki, S. Sato, N. Horimoto, T. Shimizu, S. Seino, and N. Inagaki. 2001. Protective role of ATP-sensitive potassium channels in hypoxia-induced generalized seizure. *Science.* 292:1543–1546.

Zingman, L.V., A.E. Alekseev, M. Bienengraeber, D. Hodgson, A.B. Karger, P.P. Dzeja, and A. Terzic. 2001. Signaling in channel/enzyme multimers: ATPase transitions in SUR module gate ATP-sensitive K^+ conductance. *Neuron.* 31:233–245.

Zingman, L.V., D.M. Hodgson, P.H. Bast, G.C. Kane, C. Perez-Terzic, R.J. Gumina, D. Pucar, M. Bienengraeber, P.P. Dzeja, T. Miki, et al. 2002. Kir6.2 is required for adaptation to stress. *Proc. Natl. Acad. Sci. USA.* 99:13278–13283.

1. Comparison of Mean Burst Ratios Determined by Magleby and Pallotta Method (1985) with that of Fang et al. (2006)

In this study, the mean burst duration (τ_B) was calculated using the Magleby and Palotta method (1983) from the distribution of closed times (see example in Fig. S1) using Eq. 1. In order to assess the accuracy of the mean burst ratio (BR) obtained by this method, we determined BR by an independent method, described by Fang et al. (2006). In this method, the mean burst duration τ_B is calculated as

$$\tau_B = (N+1) * \tau_O + N * \tau_F \qquad \text{(S1)}$$

where N is the number of closures within the burst, and is given by

$$N = \frac{a_f}{1 - a_f} \qquad \text{(S2)}$$

and τ_O is the mean open time, corrected for missed events calculated from the mean observed open time $\tau_{O,obs}$ as described by Davies et al. (1992):

$$\tau_O = \tau_{O,obs} * \sum_i e^{-t_d / \tau_{C,i}} \qquad \text{(S3)}$$

where t_d is "the dead time" that characterizes the resolution of the recording (determined by the filter cut-off frequency and the noise of the recording) and $\tau_{C,i}$ is the mean i^{th} closed time obtained from the fit of closed time distribution.

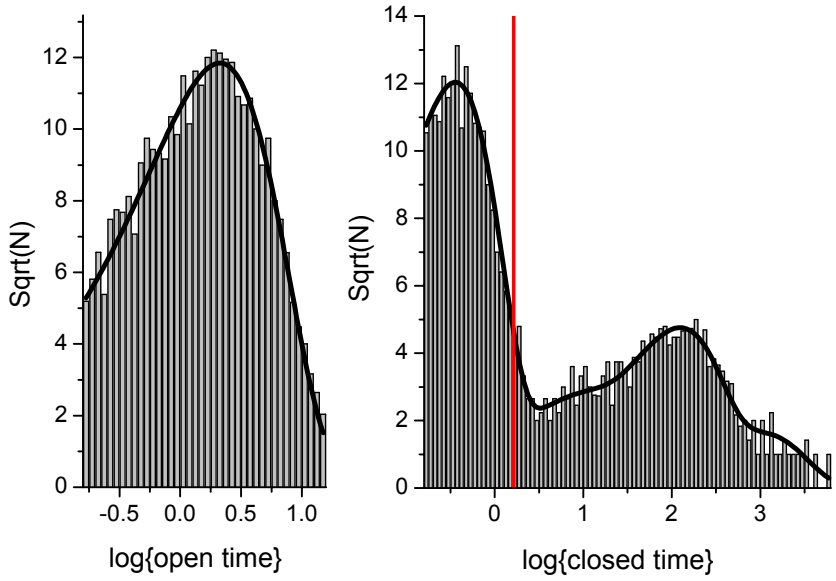

Figure S1. Example of open (left) and closed (right) time distributions (illustrated using 2WT:2M *trans* coexpressed with SUR1 and recorded at 5mM ATP). The distribution of open times is fitted with a single exponential with an observed mean open time ($\tau_{O,obs}$) of 2.11 ms. The mean open time corrected for missed events (τ_O =1.50 ms) was obtained from Eq. S3 with t_d = 0.15 ms (after Davies et al., 1992). The distribution of closed times is fitted with four exponentials with the following parameters for τ_{Ci} (mean closed time) and a_{Ci} (fractional area): τ_{C1} = 0.356 ms, a_{Ci} = 0.834; τ_{C2} = 5.84 ms, a_{C2} = 0.027; τ_{C3} = 120 ms a_{C3} = 0.123; τ_{C4} = 941 ms, a_{C4} = 0.016. The shortest component (τ_{C1}) corresponds to the short intraburst state in Scheme 1; all other components represent interburst closed times. In this example, the t_{crit} calculated using the Magleby and Palotta method (Eq. 1) is 1.64 ms (shown as the red line in Fig 1).

The burst duration calculated with this method strongly depends on the value used for the "dead time" (t_d; i.e. the shortest event it is possible to measure reliably). This value is used to calculate the corrected mean open time, from which the mean burst duration is then calculated. The value of t_d is affected by both the filter frequency and by the noise in the recordings.

In the paper, we analyzed the dwell time distributions, and the corrected mean open time, using a value for t_d = 0.15 ms. This resolution was first used by Davies et al. (1992), as well as in subsequent single-channel studies on K_{ATP} channels. If we use this value of t_d in the Fang et al. method to calculate the mean burst duration we obtain somewhat lower values of the mean burst duration than with Magleby and Pallotta's method. For example, for connected homomeric wild-type channels in the absence of ATP, the mean burst duration was 110 ± 19 ms (n = 10) using the Fang et al. method (t_d = 0.15 ms) and 127 ± 18 ms (n = 10) for the Magleby and Pallotta method.

Inspection of the dwell time histograms revealed that in our recordings, the dead time can be reduced to 0.1 ms. The use of lower values of t_d (such as the theoretical limit given by the filter frequency) clearly distorted the fit in some recordings. The mean burst duration calculated using the Fang et al. method and t_d = 0.1 ms yielded values close to those obtained using the Magleby and Pallotta method. For example, 127 ± 19 ms (n = 10) (Fang et al. method) versus 127 ± 18 ms (n = 10) (Magleby and Pallotta method), or connected homomeric wild-type channels in the absence of ATP.

We therefore used both values of t_d (0.1 ms and 0.15 ms) in the Fang et al. method to calculate the burst ratios of all tetrameric constructs and compared them with those obtained using Magleby and Pallotta method. The results are shown below. In all figures, the burst ratios and fitted lines are indicated in red for the Fang et al. method with t_d = 0.1 ms, blue for the Fang et al. method with t_d = 0.5 ms and black for the Magleby and Pallotta method.

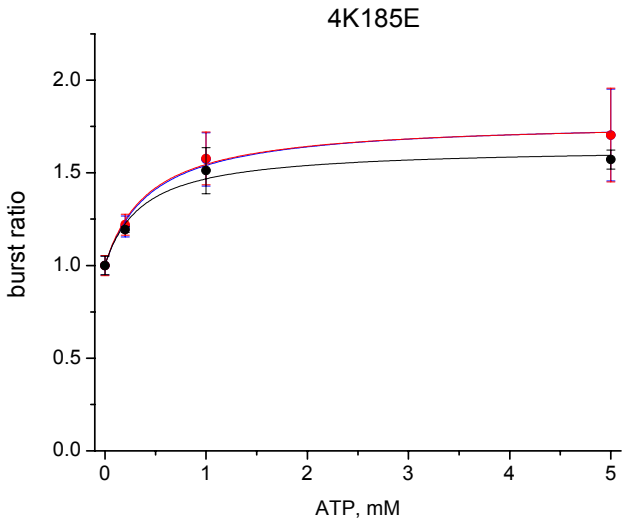

Figure S2. Connected tetramers composed of all Kir6.2-K185E subunits (with SUR1). The burst ratio was calculated using three different methods: the Fang et al. method with t_d = 0.1 ms (red circles), or t_d = 0.15 ms (blue circles), or the Magleby and Pallotta method (black circles). The lines are the best fit of Eq. 14 to the data with the following values of $K_{O,M}$ and m_M: 2.9 mM^{-1} and 1.16 (red line); 2.7 mM^{-1} and 1.16 (blue line) and $K_{O,WT}$ = 3.9 mM^{-1} and m_{WT} = 1.13 (black line, Magleby and Pallotta

method). There was no obvious difference between the data points obtained using the Fang et al. method with t_d = 0.1ms or t_d = 0.15ms (red and blue circles, see Table S1).

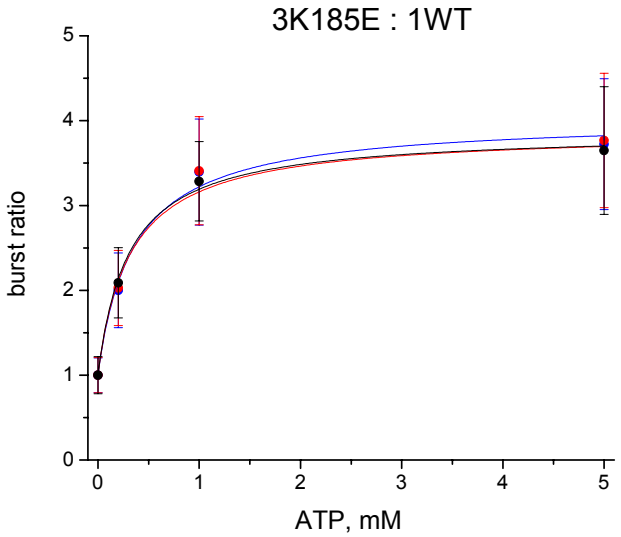

Figure S3. Connected tetramers composed of one wild-type Kir6.2 subunit and three Kir6.2-K185E subunits (with SUR1). Burst ratios were calculated using three different methods: the Fang et al. method with t_d = 0.1 ms (red circles), or t_d = 0.15 ms (blue circles), or the Magleby and Pallotta method (black circles). The lines are the best fit of Eq. 14 to the data using $K_{O,M}$ and m_M parameters obtained from the fit of connected homomeric Kir6.2-K185E channels (as shown in Fig. S2), and the following values for wild-type subunits $K_{O,WT}$ and m_{WT}: 5.5 mM^{-1} and 2.5 (red line); 4.9 mM^{-1} and 2.6 (blue line) and $K_{O,WT}$ = 4.4 mM^{-1} and m_{WT} = 2.7 (black line).

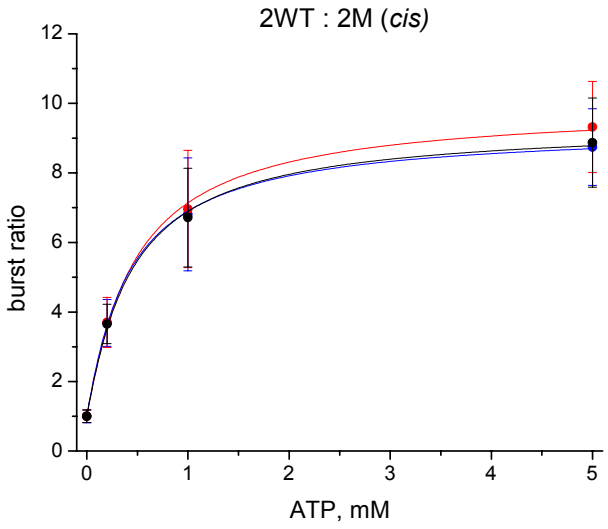

Figure S4. Connected tetramers composed of two wild-type Kir6.2 and two Kir6.2-K185E subunits (in the *cis* configuration), with SUR1. Burst ratios were calculated using three different methods: the Fang et al. method with t_d = 0.1 ms (red circles), or t_d = 0.15 ms (blue circles), or the Magleby and Pallotta method (black circles). The lines are the best fit of Eq. 14 to the data using $K_{O,M}$ and m_M parameters obtained from the fit of the homomeric mutant channels (as shown in Fig. S2) and the following values of $K_{O,WT}$ and m_{WT} for wild-type subunits: 4.2 mM^{-1} and 2.7 (red line); 4.8 mM^{-1} and 2.6 (blue line) and $K_{O,WT}$ = 4.1 mM^{-1} and m_{WT} = 2.7 (black line). There is no obvious difference between the blue and black lines (Fang et al. method with t_d = 0.15 ms and Magleby and Pallotta method).

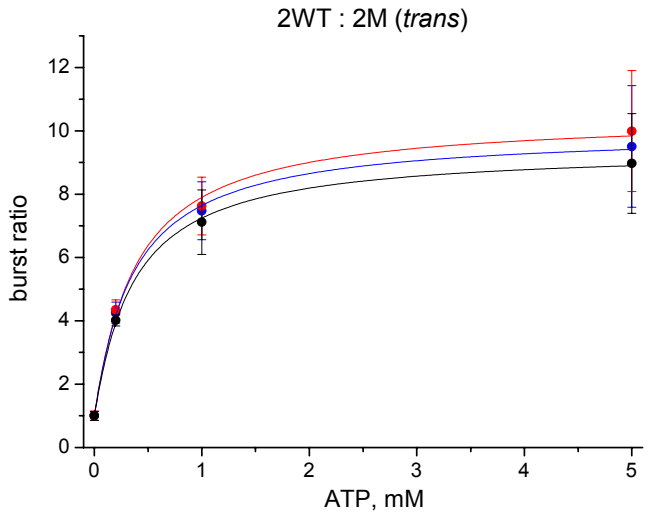

Figure S5. Connected tetramers composed of two wild-type Kir6.2 and two Kir6.2-K185E subunits (in the trans configuration), with SUR1. Burst ratios were calculated using three different methods: the Fang et al. method with t_d = 0.1 ms (red circles), or t_d = 0.15 ms (blue circles), or the Magleby and Pallotta method (black circles). The lines are the best fit of Eq. 14 to the data using $K_{O,M}$ and m_M parameters obtained from the fit of the homomeric mutant channels (as shown in Fig. S2) and following values of $K_{O,WT}$ and m_{WT} for the wild-type subunits: 5.4 mM^{-1} and 2.8 (red lines); 5.8 mM^{-1} and 2.7 (blue lines) and $K_{O,WT}$ = 5.5 mM^{-1} and m_{WT} = 2.7 (black lines).

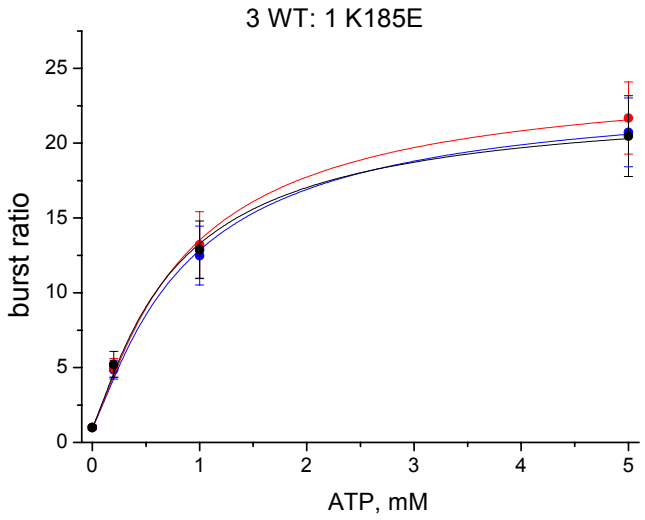

Figure S6. Connected tetramers composed of three wild-type Kir6.2 and one Kir6.2-K185 subunits. Burst ratios were calculated using three different methods: the Fang et al. method with $t_d = 0.1$ ms (red circles), or $t_d = 0.15$ ms (blue circles), or the Magleby and Pallotta method (black circles). The lines are the best fit of Eq. 14 to the data using $K_{O,M}$ and m_M parameters obtained from the fit of the homomeric mutant channels (as shown in Fig. S2) and the following values of $K_{O,WT}$ and m_{WT} for the wild-type subunits: 2.7 mM^{-1} and 2.8 (red line); 2.6 mM^{-1} and 2.7 (blue line) and $K_{O,WT} = 3.1$ mM^{-1} and $m_{WT} = 2.7$ (black line).

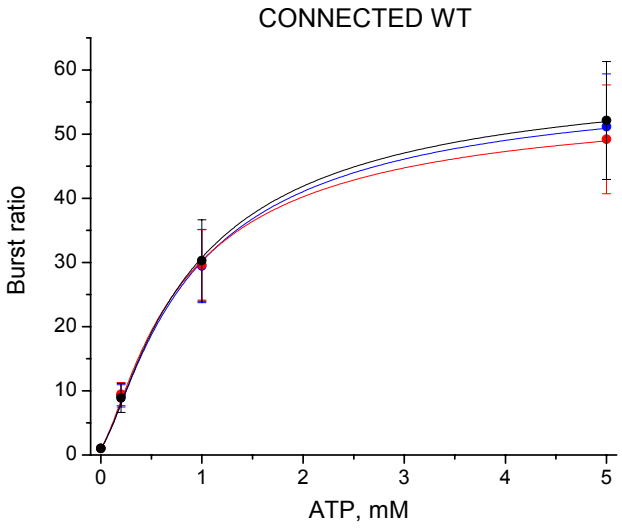

Figure S7. Connected tetramer composed of four wild-type Kir6.2 subunits, with SUR1. Burst ratios were calculated using three different methods: the Fang et al. method with t_d = 0.1 ms (red circles), or t_d = 0.15 ms (blue circles), or the Magleby and Pallotta method (black circles). The lines are the best fit of Eq. 11 to the data with the following values of $K_{O,WT}$ and m_{WT} for the wild-type subunits: 3.1 mM^{-1} and 2.7 (red line); 3.1 mM^{-1} and 2.8 (blue line) and $K_{O,WT}$ = 3.1 mM^{-1} and m_{WT} = 2.8 (black line).

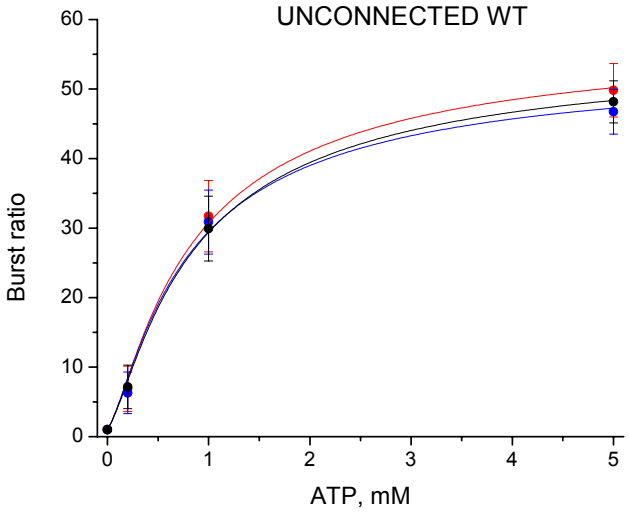

Figure S8. Unconnected tetramer composed of four wild-type Kir6.2 subunits (with SUR1). Burst ratios were calculated using three different methods: the Fang et al. method with t_d = 0.1 ms (red circles), or t_d = 0.15 ms (blue circles), or the Magleby and Pallotta method (black circles). The lines are the best fit of Eq. 11 to the data with the following values of $K_{O,WT}$ and m_{WT} for wild-type subunits: 3.3 mM^{-1} and 2.8 (red line); 3.5 mM^{-1} and 2.7 (blue line) and $K_{O,WT}$ = 3.2 mM^{-1} and m_{WT} = 2.7 (black line).

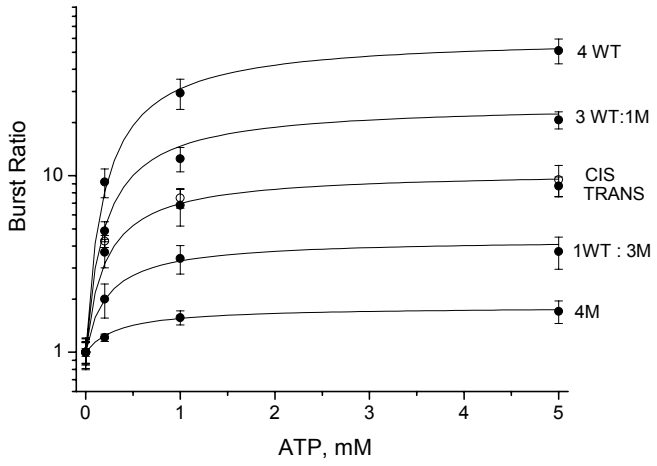

Figure S9. Mean data for all six connected tetrameric Kir6.2 constructs (coexpressed with SUR1) analyzed using the Fang et al. method with t_d = 0.15 ms. Eq. 14 was simultaneously fit to the data obtained for all six channel types. As mutant subunits make only a small contribution to heteromeric channels, $K_{O,M}$ was fixed at 2.7 mM^{-1} and m_M was fixed at 1.16 (these values were obtained from the fit of the homomeric mutant channel). The best fit yielded values of $K_{O,WT}$ = 3.1 mM^{-1} and m_{WT} = 2.8 for the wild-type subunits. These are almost indistinguishable from the values obtained when burst ratios were analyzed using the Magleby and Pallotta method ($K_{O,WT}$ = 3.2 mM^{-1} and m_{WT} = 2.7).

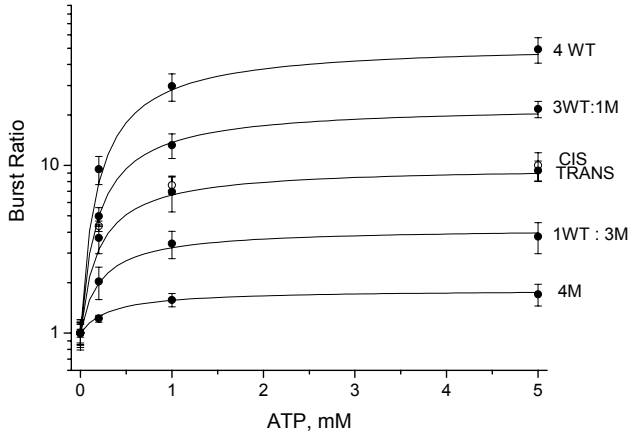

Figure S10. Mean data for all six connected tetrameric Kir6.2 constructs (coexpressed with SUR1) analyzed using the Fang et al. method with t_d = 0.1 ms. Eq. 14 was simultaneously fit to the data obtained for all six channel types. As mutant subunits make only a small contribution to heteromeric channels, $K_{O,M}$ was fixed at 2.9 mM^{-1} and m_M was fixed at 1.16 (these values were obtained from the fit of the homomeric mutant channel). The best fit yielded values of $K_{O,WT}$ = 3.3 mM^{-1} and m_{WT} = 2.7 for the wild-type subunits. These are almost indistinguishable from the values obtained when burst ratios were analyzed using the Magleby and Pallotta method ($K_{O,WT}$ = 3.2 mM^{-1} and m_{WT} = 2.7)

Construct	[ATP] (mM)	Burst ratio Fang et al. method (t_d = 0.15 ms)	Burst ratio Fang et al. method (t_d = 0.1 ms)	Burst ratio Magleby and Pallotta
connected Kir6.2-K185E	0	1.0 ± 0.1	1.0 ± 0.1	1.0 ± 0.1
	0.2	1.2 ± 0.1	1.2 ± 0.1	1.2 ± 0.1
	1	1.6 ± 0.1	1.6 ± 0.1	1.5 ± 0.1
	5	1.7 ± 0.3	1.7 ± 0.3	1.6 ± 0.1
connected 3K185E:1WT	0	1.0 ± 0.2	1.0 ± 0.2	1.0 ± 0.2
	0.2	2.0 ± 0.4	2.0 ± 0.4	2.1 ± 0.4
	1	3.4 ± 0.6	3.4 ± 0.6	3.3 ± 0.5
	5	3.7 ± 0.8	3.8 ± 0.8	3.6 ± 0.8
connected CIS	0	1.0 ± 0.2	1.0 ± 0.2	1.0 ± 0.2
	0.2	3.7 ± 0.7	3.7 ± 0.7	3.7 ± 0.6
	1	6.8 ± 1.6	6.7 ± 1.7	6.7 ± 1.4
	5	8.8 ± 1.1	9.3 ± 1.3	8.9 ± 1.3
connected TRANS	0	1.0 ± 0.1	1.0 ± 0.2	1.0 ± 0.1
	0.2	4.3 ± 0.3	4.4 ± 0.3	4.0 ± 0.2
	1	7.5 ± 0.9	7.6 ± 0.9	7.1 ± 1.0
	5	9.5 ± 1.9	10.0 ± 1.9	9.0 ± 1.6
connected 3WT: 1K185E	0	1.0 ± 0.1	1.0 ± 0.1	1.0 ± 0.2
	0.2	4.9 ± 0. 6	5.0 ± 0.6	5.2 ± 0.9
	1	12.5 ± 2.0	13.2 ± 2.2	12.9 ± 1.9
	5	20.7 ± 2.3	21.7 ± 2.4	20.5 ± 2.7
connected WT	0	1.0 ± 0.2	1.0 ± 0.2	1.0 ± 0.2
	0.2	9.2 ± 1.7	9.5 ± 1.8	8.9 ± 2.2
	1	29.4 ± 5.7	29.6 ± 5.5	30.3 ± 6.3
	5	51.2 ± 8.2	49.2 ± 8.5	52.1 ± 9.2
unconnected WT	0	1.0 ± 0.3	1.0 ± 0.3	1.0 ± 0.3
	0.2	6.3 ± 3.0	6.9 ± 3.3	7.1 ± 3.1
	1	30.9 ± 4.6	31.7 ± 5.1	29.9 ± 4.7
	5	46.7 ± 3.2	49.9 ± 3.9	48.2 ± 3.0

Table S1. Mean burst ratios of various tetrameric constructs at different ATP concentrations analyzed with three different methods. Each data point is averaged from three to five experiments.

2. ATP Sensitivity in Macroscopic and Single-Channel Recordings

Fig. S11 compares ATP concentration–inhibition curves obtained from macroscopic (filled circles; $n = 5$ in all cases) and single-channel (open circles; $n = 3–5$) recordings for connected tetramers containing different numbers of wild-type subunits: 4 (A); 3 (B); 2 cis (C); 2 trans (D); 1 (E); and 0 (F). Macroscopic data were obtained shortly after patch excision; in contrast, single-channel data were collected within 5–30 min after patch excision.

From Fig. S11 it is clear that the single-channel currents show greater ATP sensitivity than that found for the macroscopic currents. This is reflected both in the IC_{50} for channel inhibition and in the current remaining at saturating ATP concentrations (the pedestal). The greatest difference in ATP sensitivity between macroscopic and single-channel data was observed for channels with four mutant subunits (Fig. S11, E and F). In single-channel experiments, we observed that these channels also exhibited slightly faster rundown.

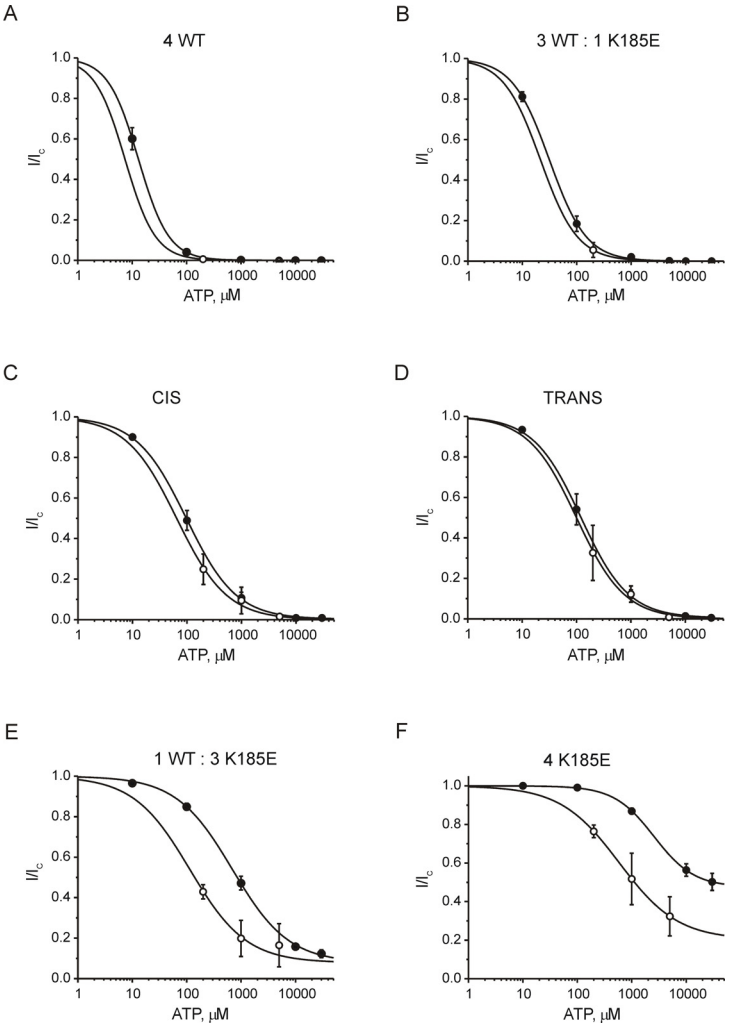

Figure S11. Comparison of ATP sensitivity in macroscopic and single-channel recordings obtained on K_{ATP} channels assembled from connected tetramers.

ATP dose–inhibition curves obtained from macroscopic (filled circles; n = 5 in all cases) and single-channel (open circles; n = 3–5) recordings for connected tetramers containing different numbers of wild-type subunits: 4 (A); 3 (B); 2 cis (C); 2 trans (D); 1 (E); and 0 (F). Data for macroscopic ATP dose–inhibition curves are identical to those in Fig. 6 A. The macroscopic data are fitted with Eq. 5 with IC_{50} = 2.6 mM, h = 1.18, p = 0.48 (0WT); IC_{50} = 690 μM, h = 0.84, and p = 0.08 (1WT); IC_{50} = 14 μM, h = 1.36, p = 0 (4WT); IC_{50} = 31 μM, h = 1.27, p = 0 (3WT); IC_{50} = 97 μM, h = 0.94, p = 0 (2cis); IC_{50} = 122 μM, h = 0.98, p = 0 (2trans).

Due to the limited number of ATP concentrations that could be applied in single-channel experiments, in most cases it was not possible to obtain reliable fits of the single-channel ATP concentration–inhibition curves with the Hill equation (Eq. 5). Thus, the data in Fig. S11 (A–D) were fit by setting the Hill coefficient *h* equal to that obtained from the corresponding macroscopic data and the pedestal value *p* in E was set to that obtained from the corresponding macroscopic data. The values of fitted parameters obtained from the fits of the single-channel data were IC_{50} = 7.4 μM (4WT), IC_{50} = 21 μM (3WT), IC_{50} = 63 μM (2cis); IC_{50} = 97 μM (2trans); IC_{50} = 95 μM; *h* = 0.71 (1WT); IC_{50} = 7.4 μM ; *h* = 0.81; *p* = 0.2 (WT).

3. ATP Dependence of BR for K_{ATP} Channels Containing Unconnected Kir6.2 Subunits

To determine to what extent the gating of connected tetramers corresponds to that of channels that lack engineered links between the subunits, we examined the single-channel properties of K_{ATP} channels with unconnected Kir6.2 subunits (Fig. S12). We recorded single-channel activity from inside-out patches excised from oocytes coinjected with SUR1 mRNA and either wild-type Kir6.2, mutant (K185E) Kir6.2, or different ratios of wild-type and mutant Kir6.2 mRNAs (Fig. S12 A). We recorded channel activity in the absence (intrinsic gating) and presence of 0.2, 1, and 5 mM ATP. In single-channel patches from oocytes coinjected with wild-type (WT) and mutant (M) mRNAs, it was possible to identify channels with kinetic signatures that resembled those observed for connected tetramers with different numbers of WT and M subunits (compare Fig. S12 A with Fig. 4).

Fig. S12 B shows that the mean BR-ATP relationship for unconnected 4WT channels (open circles) was very close to that of the connected 4WT channel (dashed line). The best fit of the data for the unconnected 4WT channel with the MWC model (Eq. 11) gave $K_{O,WT}$ = 3.25 mM^{-1} (K_d = 308 μM) and m_{WT} = 2.7. These values are very similar to those for the connected 4WT channel (K_d = 316 μM, m_{WT} = 2.8).

The BR-ATP relationship for unconnected channels was similar to that of the corresponding connected tetramers (compare Fig. 5 B with Fig. S12 B). We conclude that the linkers introduced between Kir6.2 subunits in connected tetramers do not substantially alter ATP binding to the open state (K_O) or the transduction parameter *m*. Furthermore, ATP-dependent closure of the channel pore of separate tetrameric K_{ATP} channels is also governed by the MWC mechanism.

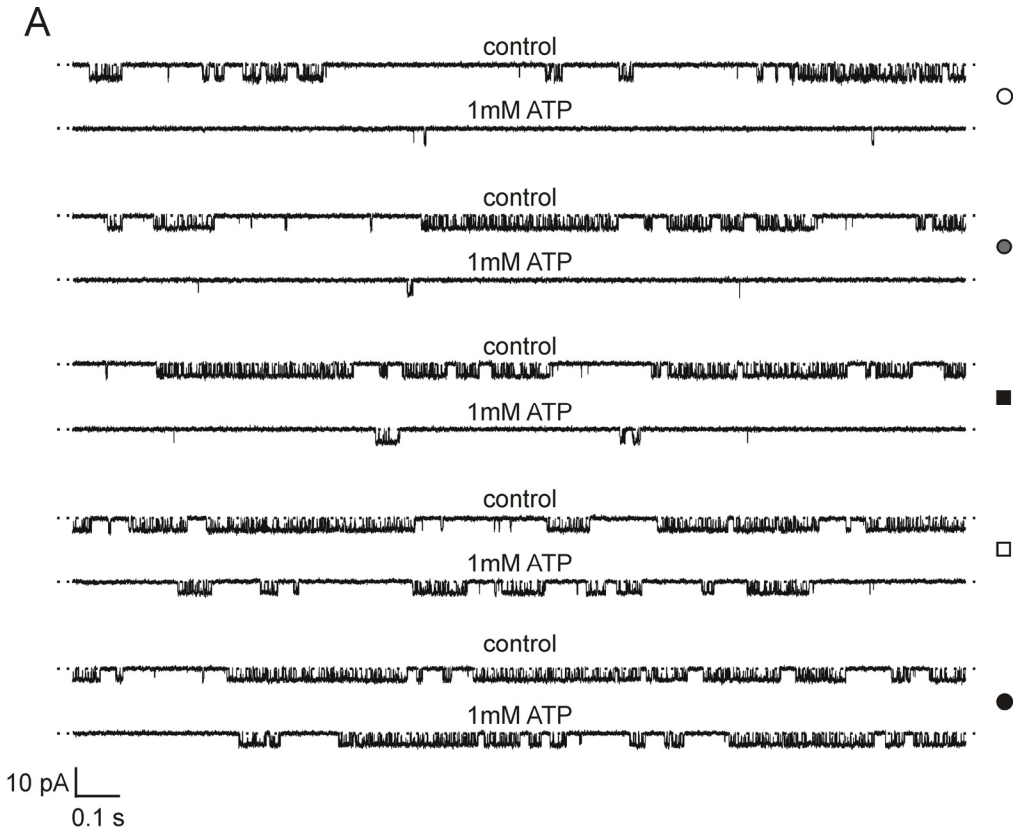
A
control
1mM ATP
control
1mM ATP
control
1mM ATP
control
1mM ATP
control
1mM ATP
10 pA
0.1 s

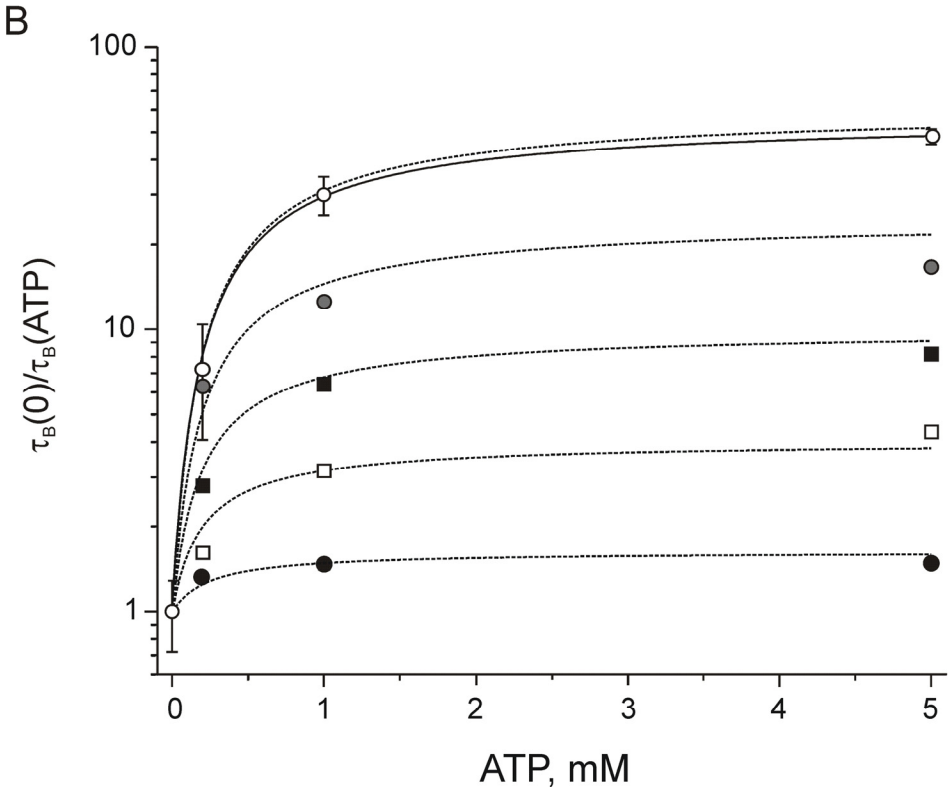
B
100
10
1
$\tau_B(0)/\tau_B(ATP)$
0
1
2
3
4
5
ATP, mM

Figure S12. The effect of ATP on BR of unconnected K_{ATP} channels. (A) Single-channel recordings at −60 mV from oocytes injected with SUR1 and different ratios of Kir6.2 and Kir6.2-K185E mRNAs in the absence and presence (1 mM) of ATP. The dotted line indicates the zero current level. Open circles: 4WT channels. Black circles: 4M channels. Grey circles: data from a single-channel patch excised from an oocyte injected with a 1:4 ratio of Kir6.2-K185E and Kir6.2 mRNAs. The data resemble connected 3WT:1M channels. Open and filled squares: data from two different single-channel patches excised from oocytes injected with SUR1 mRNA and a 4:1 ratio of Kir6.2-K185E and Kir6.2 mRNA. The data resemble connected 2WT:2M (filled squares) and 1WT:3M channels (open squares). (B) ATP dependence of the burst ratio of connected and unconnected channels plotted on a log scale. The dashed lines represent the simultaneous fit of the data from connected tetramers (Fig. 5 B) with the MWC model (Eq. 14) with $K_{O,M}$ = 3.3 mM^{-1}; m_M = 1.13 for K185E subunits and $K_{O,WT}$ = 3.1 mM^{-1}; m_M = 2.8 for wild-type subunits. The 4WT data (open circles) represent the mean of four experiments. The solid line is a best fit of the unconnected 4WT data with the MWC model (Eq. 11; $K_{O,WT}$ =3.2 mM^{-1}; m_{WT} = 2.7). The symbols are explained in A.

4. Comparison of Properties of Homomeric Wild-Type K_{ATP} Channels Formed from Connected and Separate Kir6.2 Subunits

As described in the Results, 4WT K_{ATP} channels made up of connected Kir6.2 subunits showed a substantial increase in intrinsic open probability and mean burst duration compared to unconnected 4WT channels (Fig. S13 A, also compare Fig. 4 and Fig. S12 A). Such a shift in the gating equilibrium towards the open state is expected to indirectly reduce the ATP sensitivity of the K_{ATP} channel (Trapp et al.

1998). Indeed, connected 4WT tetramers did have a slightly reduced ATP sensitivity: the IC_{50} increased from 8 to 15 μM (Fig. S13 B). This small increase in IC_{50} can be fully accounted for by the sixfold increase in the mean burst duration (Trapp et al., 1998).

Linking Kir6.2 subunits had also a dramatic effect on the ATP dependence of the mean open time τ_O (Fig. S13 C). Using Scheme 2, the reciprocal value of the mean open time is given by:

$$\frac{1}{\tau_{O,MWC}([ATP])} = a + c * \left(\frac{1 + m_{MWC} * K_{O,MWC} * [ATP]}{1 + K_{O,MWC} * [ATP]} \right)^4 \qquad \text{(S4)}$$

From this equation, it is clear that a decrease in the value of *c* will decrease the amplitude of the ATP-dependent term; in turn, this will reduce the effect of ATP on the mean open time, as observed in Fig. S13 C. A similar effect on the mean open time due to stabilization of the open state was reported for the C166S mutation (Trapp et al., 1998). Because the mean open time is a function of both intraburst and interburst closures (Scheme 2, Eq. S4) it is not possible to rearrange Eq. S4 to remove the parameter *c*, as in the case of the burst duration (Eqs. 10–12).

The reduction in the amplitude of the effect of ATP on the mean open time of the wild-type connected tetramer (Fig. S13 C) greatly reduced the accuracy with which ATP-induced changes in the mean open time could be determined: the changes were very small and comparable to the error of measurement (in most cases, ≤10% of the control value). For this reason, we could not use the ATP dependence of the mean

open time for the estimate of either K_O or m in connected channels that contained mutant subunits.

Unlike the mean burst duration and open time, the mean intraburst closed time was only mildly affected by ATP concentration (Fig. S13 D). As reported by Li et al. (2002), ATP appeared to induce a mild increase in the mean intraburst closed state duration. This effect was not substantially influenced by linking the wild-type subunits (Fig. S13 D). A similar mild increase in the intraburst closed time was observed for all concatenated constructs, suggesting that the K185E mutation does not influence ATP modulation of the intraburst closed state duration.

The mean open time, mean burst duration, and mean intraburst closed state in the absence of ATP can be used to calculate the intrinsic gating constants *a, b*, and *c* in Scheme 1 (see Eqs. 2–4 in Materials and methods). The calculated values were $a = 0.54\ ms^{-1}$, $b = 2.7\ ms^{-1}$, and $c = 0.06\ ms^{-1}$ for separated wild-type tetramers and $a = 0.59\ ms^{-1}$, $b = 2.8\ ms^{-1}$, and $c = 0.009\ ms^{-1}$ for connected wild-type tetramers, respectively.

Eq. S4 can also be used to calculate $K_{O,MWC}$ and m_{MWC} from the ATP dependence of the mean open time (Fig. S13 C). The best fit of the data yields $K_{O,MWC} = 3.2 \pm 0.2\ mM^{-1}$ ($K_d = 310 \pm 19\ \mu M$) and $m_{MWC} = 2.5 \pm 0.1$ for unconnected WT channels and $K_{O,MWC} = 3.8 \pm 0.9\ mM^{-1}$ ($K_d = 260 \pm 62\ \mu M$) and $m_{MWC} = 2.4 \pm 0.1$ for connected WT channels. These values are in good agreement with those calculated from the mean burst durations using the data shown in Figs. 5 and 6 ($K_d = 308 \pm 19\ \mu M$, m_{WT}

= 2.7 ± 0.1 and K_d = 316 ± 20 μM, m_{WT} = 2.8 ± 0.1 for unconnected and connected 4WT channels, respectively).

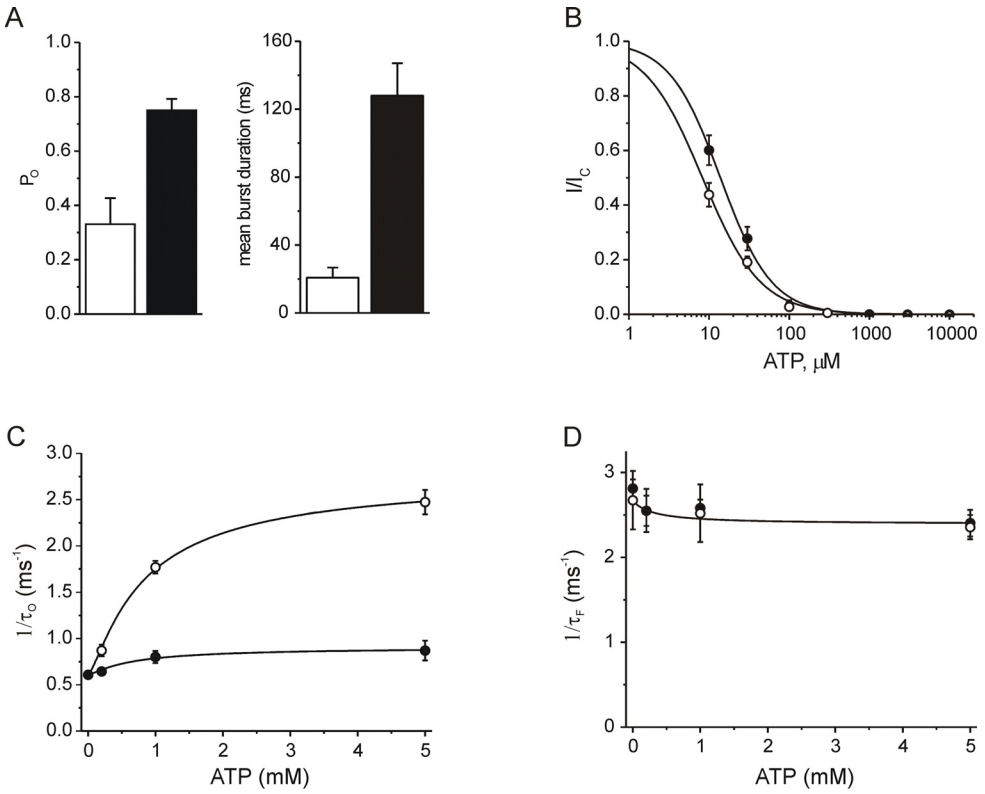

Figure S13. Comparison of properties of unconnected and connected homomeric wild-type K_{ATP} channels. (A) Mean open probability and burst duration in the absence of ATP unconnected (white circles, n = 10) and connected K_{ATP} channels (black circles, n = 10). In B–D, open symbols refer to unconnected K_{ATP} channels and solid symbols to connected K_{ATP} channels. (B) Dose–response curve for ATP inhibition of unconnected (n = 5) and connected wild-type K_{ATP} channels (n = 5). The lines are best fit of the data to Eq. 5 were obtained with IC_{50} = 8.3 μM and h = 1.20 and IC_{50} = 13.9 μM and h = 1.36 for unconnected and connected channels, respectively. (C) Mean open time dependence on ATP (each data point is the mean of three to five experiments). The lines are best fit of Eq. S4 to the data with $K_{O,MWC}$ = 3.2 mM^{-1}; m_{MWC} = 2.5 for unconnected wild-type channels and $K_{O,MWC}$ = 3.8 mM^{-1}; m_{MWC} = 2.4 for connected wild-type tetramers. (D) Dependence of the mean intraburst closed

duration on ATP concentration. The line is the best fit of the data on unconnected wild-type channels with the equation:

$$\frac{1}{\tau_{F,MWC}} = b * \left(\frac{1 + q_{MWC} * K_{F,MWC} * [ATP]}{1 + K_{F,MWC} * [ATP]} \right)^4 \quad \text{(S5)}$$

where q_{MWC} = 0.97, b = 2.7 ms^{-1}, and $K_{F,MWC}$ was assumed to be identical to that of the open state ($K_{O,MWC}$) and fixed at 3.2 mM^{-1}.